

Charged lepton flavor violation associated with heavy quark production in deep inelastic lepton-nucleon scattering via scalar exchange

Yuichiro Kiyo,^{1,*} Michihisa Takeuchi,^{2,†} Yuichi Uesaka,^{3,‡} and Masato Yamanaka^{4,5,§}

¹*Department of Physics, Juntendo University, Inzai, 270-1695 Japan*

²*Department of Physics, Osaka University, Osaka 560-0043, Japan*

³*Faculty of Science and Engineering,
Kyushu Sangyo University, 2-3-1 Matsukadai,
Higashi-ku, Fukuoka 813-8503, Japan*

⁴*Department of Mathematics and Physics,
Osaka City University, Osaka 558-8585, Japan*

⁵*Nambu Yoichiro Institute of Theoretical and Experimental Physics (NITEP),
Osaka City University, Osaka 558-8585, Japan*

(Dated: June 12, 2025)

Abstract

We study charged lepton flavor violation (CLFV) associated with heavy quark pair production in lepton-nucleon deep-inelastic scattering $\ell_i N \rightarrow \ell_j q \bar{q} X$. Here ℓ_i and ℓ_j denote the initial and final leptons, N and X are the initial nucleon and arbitrary final hadronic system, respectively. We employ a model Lagrangian in which a scalar and pseudoscalar mediator generate the CLFV. We derive heavy quark structure functions for scalar and pseudoscalar currents and compute momentum distributions of the final lepton for the process. Our focus is on the heavy quark mass effects in the final lepton momentum distribution. We clarify a necessity of inclusion of the heavy quark mass to rise a sensitivity of search for charged lepton flavor violation in the deep inelastic scattering.

*E-mail: ykiyo@juntendo.ac.jp

†E-mail: m.takeuchi@het.phys.sci.osaka-u.ac.jp

‡E-mail: uesaka@ip.kyusan-u.ac.jp

§E-mail: yamanaka@osaka-cu.ac.jp

I. INTRODUCTION

A variety of new physics models provides contributions to the Charged Lepton Flavor Violating (CLFV) observables by extra degrees of freedom, for instance extensions of particle contents, additional space dimensions, etc. For the reviews on the CLFV, see [1, 2]. It is often the case that the CLFV mediators couple with not only leptons, but also quarks. In that case, noticeable processes which involve hadronic interactions, e.g., $\mu \rightarrow e$ conversion in nuclei, $\tau \rightarrow \ell_i \pi \pi$ ($\ell_i = e, \mu$), different flavor di-lepton $\ell_i \ell_j$ production at hadron collider experiments, would be expected. No signal for such types of the CLFV processes is discovered so far although a lot of effort to search for them has been devoted in the various experiments. These results are translated into the stringent limits on the CLFV interactions, however, mainly on the interactions related with light flavor quarks. This motivates us to revisit the scenarios where the CLFV mediators dominantly couples with heavy quarks. Such scenarios are motivated theoretically as well as experimentally, e.g. extra-dimension models [3–6], two Higgs doublet models [7–9], leptoquark models, and models with flavor symmetry [10]. In such scenarios, the CLFV process via deep-inelastic scattering (DIS) $eN \rightarrow \ell' X$ where N is a nucleon and $\ell' = \mu, \tau$ offers a good prospect. Such a process are probed at fixed target experiments and at lepton-hadron colliders. In this manuscript, we focus on the prospect at the fixed target experiments. The event rate in such a experiment increases with the beam energy, beam intensity and the target density. A typical beam energy in the next-generation experiments is up to $E_\ell \lesssim 10\text{TeV}$, which corresponds to $\sqrt{s} \lesssim 100\text{GeV}$. Although it seems not high, it is sufficient to open the production threshold of CLFV signals. Therefore it is expected to produce enough signals of the CLFV. Note that, in fixed target experiments or in lepton-hadron collider experiments, the problems due to pile-up and QCD background are better-controlled than in the environments of the hadron-hadron colliders.

The DIS processes are studied with a variety of theoretical motivations in the context of the CLFV [11–23], as well as a probe for the Standard Model (SM) and new physics [24–33]. The HERA experiment searched for the CLFV DIS processes and put the bound on the related parameters [34, 35]. Searches for the CLFV DIS processes are proposed at the upcoming experiments, and shown to reach higher sensitivities than the current bounds by a few orders of magnitude [36, 37].

In this manuscript, we study the CLFV DIS processes, $\ell_i N \rightarrow \ell_j X_H$, in the scenario where a (pseudo-)scalar CLFV mediator dominantly couples with heavy flavor quarks, like the SM Higgs boson. Here X_H denotes an inclusive hadronic final state involving heavy quarks. It is worth investigating the CLFV DIS processes associated with heavy flavor quarks, since the CLFV operators involving heavy flavor quarks are usually difficult to probe directly in the low energy flavor experiments. Experimental signals for the processes are characterized as the existence of a heavy charged lepton ℓ_j and heavy quarks in the final state. Such signals seem distinctive, but there is always a competition between the signals and the background. Thus, the precise knowledge of the backgrounds and also the accurate theory prediction for the signal processes would be required. In this manuscript, we focus on the latter point. One of differences between heavy quarks and light quarks is the mass effect, and it is important to understand how the heavy quark mass affects the CLFV DIS observables. At first glance,

this sounds simple and straightforward, nevertheless it turns out rather complicated when the issue is related to the problem of the large logarithmic resummation in the perturbative QCD. A resolution to the problem was given in a seminal paper by ACOT [38] at LO, and the result has been extended to include higher order effect in a consistent manner [39, 40]. In the present paper we apply the ACOT method to the CLFV DIS involving heavy quarks. Although we work at LO in QCD strong coupling expansion in the present paper, we include some of the important effects which were obtained in the studies of QCD structure functions for heavy quark productions. We aim for a construction of heavy quark structure functions of (pseudo-)scalar exchange coming from CLFV interactions. With the constructed heavy quark structure functions we analyze some distributions of the final lepton momentum to investigate how the heavy quark mass effect modifies the CLFV DIS observables. We focus on the analysis of the CLFV DIS processes associated with heavy quark production in the present paper, and a comprehensive phenomenological study taking other modes will be reported in a separate paper.

II. CLFV DIS AND HEAVY QUARK PRODUCTION

A. CLFV DIS via scalar or pseudoscalar current

We start with an interaction Lagrangian for a neutral scalar or pseudoscalar field $\phi = \phi_S, \phi_P$ coupled with charged leptons ℓ_i and heavy flavor quarks $q = c, b, t$;

$$\mathcal{L}_\phi = - \sum_{ij} \left(\rho_{ij}^\phi \bar{\ell}_j P_L \ell_i \phi + h.c. \right) - \sum_q \rho_{qq}^\phi \bar{q} \Gamma^\phi q \phi, \quad \phi \in \{\phi_S, \phi_P\} \quad (1)$$

where i, j run over flavor indices of charged leptons, q runs over heavy quark flavors, $P_L = (1 - \gamma_5)/2$, and $\Gamma^{\phi_S} = 1, \Gamma^{\phi_P} = i\gamma_5$ is a matrix in Dirac-space respectively for scalar or pseudoscalar cases. The lepton and quark fields in the interaction Lagrangians are mass eigenstates. We assume that the CLFV mediators interact with quarks through flavor diagonal couplings ρ_{qq}^ϕ while in the lepton sector the off-diagonal coupling $\rho_{ij}^\phi (i \neq j)$ induces the CLFV.

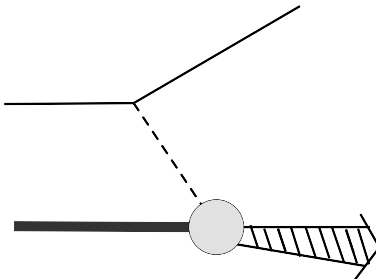


FIG. 1: CLFV lepton-nucleon scattering: The initial and final lepton momenta are k_i and k_j , respectively, and the nucleon momentum is P .

In Fig.1 schematic diagram for the process $\ell_i N \rightarrow \ell_j X_H$ is shown, where initial lepton ℓ_i with a momentum k_i and a nucleon N with a momentum P are scattered by exchanging CLFV mediator ϕ with a momentum $q = k_i - k_j$. The final states are lepton ℓ_j with momentum k_j and arbitrary hadronic systems X_H which contains heavy quarks. The CLFV amplitude where the CLFV mediator ϕ is exchanged in t -channel is factorized into leptonic and hadronic amplitudes. The cross section σ consists of leptonic and hadronic parts, which is respectively denoted by L_ϕ and F_ϕ , and written in the following form

$$\frac{d\sigma}{dx dy}(\ell_i N \rightarrow \ell_j X) = \frac{y |\rho_{qq}^\phi|^2 L_\phi(Q^2) F_\phi(x, Q^2)}{16\pi (Q^2 + m_\phi^2)^2}, \quad (2)$$

where m_ϕ is a mediator mass, and the dimensionless variables x, y are defined by

$$x = \frac{Q^2}{2P \cdot q}, \quad y = \frac{2P \cdot q}{2P \cdot k_i}, \quad (3)$$

with $Q^2 = -q^2 = xy(s - m_N^2)$. Here $s = (P + k_i)^2$ is collision energy squared of initial lepton-nucleon system, and m_N is the nucleon mass.

The leptonic part is given by

$$L_\phi = (|\rho_{ij}^\phi|^2 + |\rho_{ji}^\phi|^2)(Q^2 + m_i^2 + m_j^2) + 4 \text{Re}(\rho_{ij}^\phi \rho_{ji}^\phi) m_i m_j, \quad (4)$$

with $m_{i(j)}$ being the initial (final) lepton mass, and the hadronic part is called structure function written in a convolution form as

$$F_\phi(x, Q^2) = \sum_k \int_0^1 \frac{d\xi}{\xi} C_k\left(\frac{x}{\xi}\right) f_{k/N}(\xi, \mu_f^2). \quad (5)$$

where $k \in \{g, q, \bar{q}\}$ is a parton which contributes to the process $\phi k \rightarrow X$. The C_k is coefficient function calculable in perturbative QCD, while parton distribution function (PDF) $f_{k/N}(x, \mu_f^2)$ is a nonperturbative object which describes a probability of parton i having momentum fraction ξ inside the nucleon N at a factorization scale μ_f . The μ_f dependence is governed by renormalization group equation, so called Dokshitzer-Gribov-Lipatov-Altarelli-Parisi (DGLAP) equation [41, 42] :

$$\mu_f^2 \frac{\partial}{\partial \mu_f^2} f_{k/N}(\xi, \mu_f^2) = \sum_l \frac{\alpha_s(\mu_f^2)}{2\pi} \int_\xi^1 \frac{d\eta}{\eta} \mathcal{P}_{kl}\left(\frac{\xi}{\eta}\right) f_{l/N}(\xi, \mu_f^2) + \mathcal{O}(\alpha_s^2), \quad (6)$$

where l runs over possible quark flavors and gluon, and \mathcal{P}_{kl} is a splitting function at one-loop level. Conventionally (and also in our phenomenological analysis) the factorization scale is chosen as $\mu_f^2 \sim Q^2$. In the present work we use CT14LO PDFs [43].

B. Cross sections and distribution

In theory discussion it is sometimes convenient to use x, Q^2 as independent variables instead of x, y . The conversion formula is given by

$$\frac{d^2\sigma}{dx dQ^2}(\ell_i N \rightarrow \ell_j X) = \left(\frac{1}{xs}\right) \frac{d^2\sigma}{dx dy}(\ell_i N \rightarrow \ell_j X). \quad (7)$$

Integrated over x one obtain the differential cross section $d\sigma/dQ^2$ as

$$\frac{d\sigma}{dQ^2} = \frac{|\rho_{qq}^\phi|^2}{16\pi s^2} \frac{Q^2 L_\phi(Q^2) M_\phi(s, Q^2)}{(Q^2 + m_\phi^2)^2}, \quad (8)$$

where M_ϕ is the second inverse moment of the structure function defined by

$$M_\phi(s, Q^2) \equiv \int_{x_{\min}(s, Q^2)}^{x_{\max}(Q^2)} x^{-2} F_\phi(x, Q^2) dx. \quad (9)$$

The integration region $[x_{\min}(s, Q^2), x_{\max}(Q^2)]$ depends on partonic processes, and the $x_{\min}(s, Q^2)$ depends on s , which introduces the collider energy dependence of the inverse moment. A derivation of the physical region in CLFV DIS is given in the Appendix.

As a direct observable in collider experiment, we study a momentum distribution of final lepton. To make our discussion concrete we give a cross section formula for $eN \rightarrow \tau X$ for fixed target experiment where the initial nucleon is at the rest. The initial nucleon and electron momentum is parametrized by $k_e = (E_e, 0, 0, E_e)$ and $P = (m_N, 0, 0, 0)$, respectively. Here we ignored the electron mass. The τ -momentum at the nucleon rest frame is parametrized as $k_\tau = (E_\tau, p_T, 0, p_Z)$ where p_T, p_Z are related to dimensionless parameters x, y as

$$p_Z = (1 - y)E_e - xy m_N - \frac{m_\tau^2}{2E_e}, \quad p_T = \sqrt{(1 - y)^2 E_e^2 - m_\tau^2 - p_Z^2}, \quad (10)$$

and $E_\tau = (1 - y)E_e$. The differential cross section at the nucleon rest frame is given by

$$\frac{d^2\sigma}{dp_T dp_Z}(\ell_i N \rightarrow \ell_j X) = \left[\frac{2p_T}{E_\tau y(s - m_N^2)} \right] \frac{d^2\sigma}{dx dy}(\ell_i N \rightarrow \ell_j X), \quad (11)$$

where a Jacobian factor is multiplied in the right-hand side of Eq.(11) to convert the independent variables from (x, y) to (p_T, p_Z) .

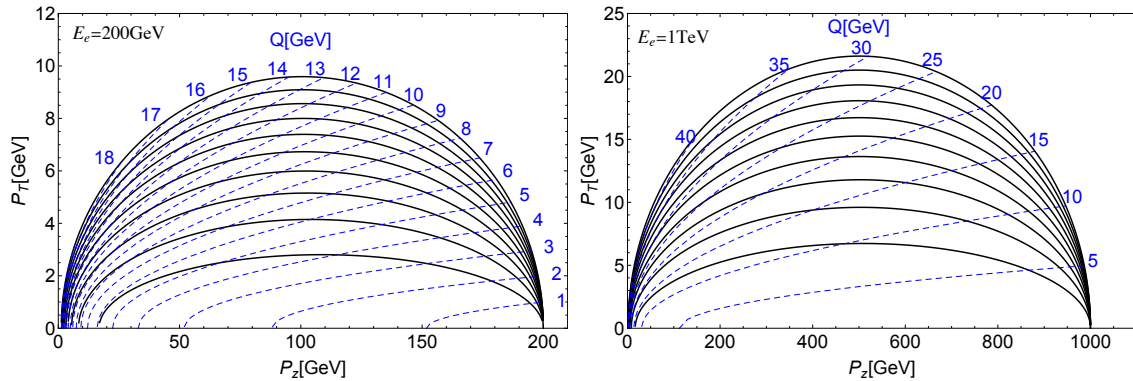


FIG. 2: Contour lines of fixed x (black lines) and fixed Q (dashed blue lines) are plotted in the τ -lepton momentum space (p_z, p_T) .

In Fig.2 physical region of τ -momentum (p_z, p_T) is plotted for the beam energies $E_e = 200\text{GeV}$ and 1TeV respectively in left and right panels. The black lines are contours for fixed

x -value for $x = 0.1, 0.2, \dots, 1$, and blue dashed lines are contour lines for specific values of Q . For CLFV signal searches in fixed target experiments it is of great importance to have a reliable theory prediction which covers all the physical region of Fig.2. This means that we want to have a reliable theory scheme which covers wide region of (x, Q) .

C. Heavy quark contribution to structure function

In the following we consider heavy quark production due to CLFV scalar or pseudoscalar interactions. To be concrete we assume that the heavy quark q is bottom or charm quark, which is much heavier than the nucleon, and other quarks as massless. The heavy quark mass is so large that its intrinsic partonic content inside the nucleon is zero. Yet the heavy quark can be produced in pair with its anti-quark via a gluon splitting $g \rightarrow q\bar{q}$ and subsequently q or \bar{q} is scattered by $\phi = S, P$ via quark-mediator interaction of \mathcal{L}_ϕ . In Fig. 3 an example Feynman diagram is shown for such a process.

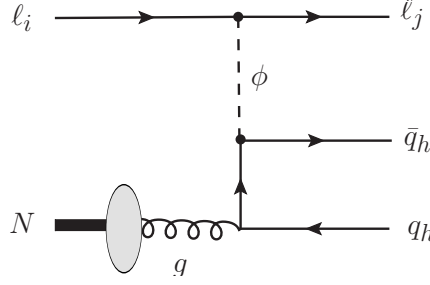


FIG. 3: A Feynman diagram for the heavy quark pair production in CLFV lepton-nucleon scattering.

The corresponding hadronic part F_ϕ which contributes to the $\ell_i N \rightarrow \ell_j q \bar{q} X$ is given by

$$F_\phi^M(x, Q^2) = \int_0^1 \frac{d\xi}{\xi} C_g^M\left(\frac{x}{\xi}, \frac{Q^2}{m_q^2}\right) f_{g/N}(\xi, \mu_f^2), \quad (12)$$

where C_g^M is a heavy quark contribution to the coefficient function. The super-script M indicates that the quantity is computed in massive scheme, where the heavy quark mass is retained in the computation:

$$C_g^M\left(\frac{x}{\xi}, \frac{Q^2}{m_q^2}\right)\Big|_S = \frac{\alpha_s}{2\pi} \frac{T_F}{(Q^2 + w^2)^2} \Theta(w^2 - 4m_q^2) \left\{ 2Kw^2(Q^2 + 4m_q^2) + \left[Q^2(Q^2 + 4m_q^2) + (w^2 - 4m_q^2)^2 \right] \ln \frac{1+K}{1-K} \right\}, \quad (13)$$

$$C_g^M\left(\frac{x}{\xi}, \frac{Q^2}{m_q^2}\right)\Big|_P = \frac{\alpha_s}{2\pi} \frac{T_F}{(Q^2 + w^2)^2} \Theta(w^2 - 4m_q^2) \left\{ 2Kw^2Q^2 + \left[Q^2(Q^2 + 4m_q^2) + w^4 \right] \ln \frac{1+K}{1-K} \right\} \quad (14)$$

with $T_F = 1/2$, the Heaviside step function $\Theta(x)$. The $K = \sqrt{1 - 4m_q^2/w^2}$ is relative velocity of heavy quark pair with $w^2 = (q + \xi P)^2 = Q^2(\xi/x - 1)$ being the invariant mass of $q\bar{q}$. Thus, the step function can be rewritten as $\Theta(w^2 - 4m_q^2) = \Theta(\xi - \chi)$ with $\chi \equiv \left(1 + \frac{4m_q^2}{Q^2}\right)x$. Appearance of χ , not x , is an important mass effect due to the pair production threshold of $q\bar{q}$. This leads χ -rescaling prescription [44, 45] based on an idea of so-called slow-rescaling [46], which will be discussed later.

D. SACOT scheme



FIG. 4: Feynman diagrams for the heavy quark pair production (a), and heavy quark excitation diagram(b).

In Eqs. (13) and (14), the heavy quark contribution to the coefficient function is calculated retaining the heavy quark mass, which corresponds to the left panel (a) of Fig. 4, and its behavior around the threshold $w^2 \sim 4m_q^2$ is correctly described order by order in perturbative expansion of α_s . However when $Q^2 \gg m_q^2$ there appears a large logarithm $\ln(Q^2/m_q^2)$, and its appearance deteriorates the perturbative computation of C_g^M . It can be seen by expanding C_g^M in the limit $(m_q^2/Q^2) \rightarrow 0$:

$$C_g^M \approx \int_0^1 \frac{d\eta}{\eta} \left[C_q^{\text{ZM}}\left(\frac{x}{\eta}\right) + C_{\bar{q}}^{\text{ZM}}\left(\frac{x}{\eta}\right) \right] \Theta(\xi - \eta) \left[\left(\frac{\alpha_s}{2\pi}\right) \mathcal{P}_{qg}\left(\frac{\eta}{\xi}\right) \ln\left(\frac{Q^2}{m_q^2}\right) \right], \quad (15)$$

where $\mathcal{P}_{qg}(z) = T_F[z^2 + (1-z)^2]$ is a gluon-quark splitting function, and $C_q^{\text{ZM}}(x) = C_{\bar{q}}^{\text{ZM}}(x)$ are single heavy quark contributions to the coefficient function in the massless limit, corresponding to the right diagram of Fig. 4:

$$C_q^{\text{ZM}}(x) = \frac{1}{2} \delta(1-x). \quad (16)$$

Therefore the high energy limit of the structure function can be written as

$$F_\phi^{\text{M0}}(x, Q^2) = \int_0^1 \frac{d\eta}{\eta} 2C_q^{\text{ZM}}\left(\frac{x}{\eta}\right) \frac{\alpha_s}{2\pi} \ln\left(\frac{\mu_f^2}{m_q^2}\right) \int_\eta^1 \frac{d\xi}{\xi} \mathcal{P}_{qg}\left(\frac{\eta}{\xi}\right) f_{g/N}(\xi, \mu_f^2) \quad (17)$$

where the superscript M0 denotes the leading contribution in the massless limit of the massive scheme structure function. Namely the F_ϕ^{M0} contains the mass singularity of the massive structure function, and $(F_\phi^M - F_\phi^{\text{M0}})$ is finite in the massless limit. Here, the original collinear logarithm existing in Eq.(15) is separated as $\alpha_s \ln(Q^2/m_q^2) = \alpha_s \ln(Q^2/\mu_f^2) + \alpha_s \ln(\mu_f^2/m_q^2)$, and the mass singularity $\alpha_s \ln(\mu_f^2/m_q^2)$ is absorbed in Eq.(17).

The relation between the high energy limit of massive quark contribution and F_ϕ^{M0} structure function is nothing but the factorization theorem of collinear singularity for QCD structure function, which can be utilized to resum the large collinear logarithms to all order in α_s to make the cross section stable even at high energy. The extracted collinear logarithm $\alpha_s \ln(\mu_f^2/m_q^2)$ has a form, that can be resummed to all orders in α_s by means of DGLAP evolution equation, leading to zero mass (ZM) scheme structure function F_ϕ^{ZM} :

$$\begin{aligned} F_\phi^{\text{ZM}}(x, Q^2) &= \int_0^1 \frac{d\eta}{\eta} 2C_q^{\text{ZM}}\left(\frac{x}{\eta}\right) [f_{q/N}(\eta, \mu_f^2) + f_{\bar{q}/N}(\eta, \mu_f^2)] \\ &= \frac{1}{2} [f_{q/N}(x, \mu_f^2) + f_{\bar{q}/N}(x, \mu_f^2)]. \end{aligned} \quad (18)$$

The heavy quark PDFs $f_{q/N}$ and $f_{\bar{q}/N}$ introduced in Eq.(18) are generated by gluon splitting into $q\bar{q}$ through the DGLAP evolution equation, and thus reduces to Eq.(17) at leading order in the α_s expansion:

$$f_{q/N}(x, \mu_f^2) = \frac{\alpha_s}{2\pi} \ln\left(\frac{\mu_f^2}{m_q^2}\right) \int_x^1 \frac{d\xi}{\xi} \mathcal{P}_{qg}\left(\frac{x}{\xi}\right) f_{g/N}(\xi, \mu_f^2) + \mathcal{O}(\alpha_s^2). \quad (19)$$

So far we defined three types of structure function F_ϕ^{M} , F_ϕ^{M0} and F_ϕ^{ZM} . The M-scheme structure function is reliable in low Q^2 region but unreliable in high Q^2 region due to the mass singularity, while the ZM scheme structure function is reliable in high Q^2 region but unreliable in low Q^2 region. Therefore these two are complementary to each other. According to these observations a scheme for the structure function was constructed, which includes heavy quark mass effects near $q\bar{q}$ threshold region and also the large logarithm resummation making the cross section stable even at high Q^2 region. The result is a new structure function which consists of three terms as

$$F_\phi^{\text{SACOT}}(x, Q^2) = F_\phi^{\text{M}}(x, Q^2) + F_\phi^{\text{ZM}}(x, Q^2) - F_\phi^{\text{sub}}(x, Q^2). \quad (20)$$

Here the second and third terms are computed by setting heavy quark masses to zero, and this is called Simplified ACOT (SACOT) scheme [38, 47]. The first term F_ϕ^{M} is the contribution of heavy quark pair to the structure function where heavy quarks q, \bar{q} are massive and produced by gluon splitting. The second term F_ϕ^{ZM} plays a role to resum the large-collinear logarithm $\ln(Q^2/m_q^2)$ to all orders in α_s by use of the heavy quark and anti-quark PDFs $f_q(x, \mu_f^2)$. By construction of F_ϕ^{ZM} , there is a double counting of large-logarithm between F_ϕ^{M} and F_ϕ^{ZM} , and this double counting effect should be subtracted by the last term:

$$F_\phi^{\text{sub}}(x, Q^2) = F_\phi^{\text{M0}}(x, Q^2). \quad (21)$$

Physical picture of the SACOT scheme is as follows: the first term F_ϕ^{M} contains all the mass effects order by order in α_s -expansion, and the second term add the large logarithmic corrections to improve Q^2 range avoiding the double counting by the last term.

E. Improvements for threshold behavior

Although we are working on the leading order formulations for the heavy quark structure functions, there is a numbers of important higher effects on the threshold behavior of the structure functions. We take into account such improvements here.

The first such effect is one by so-called χ -rescaling prescription. The χ -rescaling prescription aims to incorporate threshold kinematics of heavy quark production into the massless structure function (ZM) and massless limit (M0) of massive structure functions using $\chi(x, Q^2) = (1 + Q^2/4m_q^2)x$ instead of x variable. This defines structure functions in ZM- χ and M0- χ schemes:

$$F_\phi^{\text{ZM-}\chi}(x, Q^2) = \frac{1}{2} [f_{q/N}(\chi(x, Q^2), \mu_f^2) + f_{\bar{q}/N}(\chi(x, Q^2), \mu_f^2)], \quad (22)$$

$$F_\phi^{\text{M0-}\chi}(x, Q^2) = \frac{\alpha_s}{2\pi} \ln\left(\frac{\mu_f^2}{m_q^2}\right) \int_{\chi(x, Q^2)}^1 \frac{d\xi}{\xi} \mathcal{P}_{qg}\left(\frac{\chi(x, Q^2)}{\xi}\right) f_{g/N}(\xi, \mu_f^2). \quad (23)$$

The subtraction term with χ -rescaling is similarly defined by $F_\phi^{\text{sub-}\chi}(x, Q^2) = F_\phi^{\text{M0-}\chi}(x, Q^2)$. With above structure functions SACOT- χ scheme is also defined as

$$F_\phi^{\text{SACOT-}\chi}(x, Q^2) \equiv F_\phi^{\text{M}}(x, Q^2) + [F_\phi^{\text{ZM-}\chi}(x, Q^2) - F_\phi^{\text{sub-}\chi}(x, Q^2)]. \quad (24)$$

The second improvement is a choice of the factorization scale μ_f . In the traditional DIS analysis the scale choice $\mu_f^2 = Q^2$ is commonly used. However a low scale value where $\mu_f^2 = Q^2 \ll m_q^2$ is not favorable for the heavy quark production. To ensure that the factorization scale does not become too low we take factorization scale as

$$\mu_Q^2 = Q^2 [c(1 - z_m)^n \Theta(1 - z_m) + z_m], \quad (25)$$

where $z_m = m_q^2/Q^2$, $n = 2$ and $c = 0.5$ are chosen following Ref.[38].

The last improvement applies on the SACOT structure function. The SACOT structure function interpolates between massive and massless structure functions, F_ϕ^{M} and F_ϕ^{ZM} . Ideally F^{SACOT} is supposed to reduce to the massive one in low- Q^2 region, while in high- Q^2 region to the massless one. This expectation holds true parametrically at each order in perturbative expansion, but numerically F_ϕ^{SACOT} does not converge to F_ϕ^{M} near heavy quark threshold $Q^2 \sim m_q^2$. This is because the cancellation between F_ϕ^{ZM} and F_ϕ^{sub} in low Q^2 region is not effective due to unsuppressed higher order terms in α_s resummed into F_ϕ^{ZM} . Namely the terms $F_\phi^{\text{ZM}} - F_\phi^{\text{M0}} = \mathcal{O}(\alpha_s^k L^k)$ ($k \geq 2$) are too large in the region where the massless approximation is not trustable. Easy solution to avoid this trouble is to suppress the $F_\phi^{\text{ZM}} - F_\phi^{\text{sub}}$ in low Q^2 region by hand. Thus we define improved structure functions for ZM- χ and M0- χ schemes: in threshold behavior as

$$F_{\phi, \text{thr}}^{\text{ZM-}\chi}(x, Q^2) = F_\phi^{\text{ZM-}\chi}(x, Q^2) S_{\text{thr}}(m_q^2/Q^2), \quad (26)$$

$$F_{\phi, \text{thr}}^{\text{M0-}\chi}(x, Q^2) = F_{\phi, \text{thr}}^{\text{sub-}\chi}(x, Q^2) = F_\phi^{\text{M0-}\chi}(x, Q^2) S_{\text{thr}}(m_q^2/Q^2), \quad (27)$$

where $S_{\text{thr}}(m_q^2/Q^2)$ is a function which suppress the structure functions in ZM- χ and M0- χ schemes forcing them to smoothly match with correct threshold behavior. The func-

tional form of $S_{\text{thr}}(z)$ is somewhat arbitrary but only requirement is $S_{\text{thr}}(z) \xrightarrow{z \rightarrow 0} 1$ for large-logarithm resummation. For simplicity we choose

$$S_{\text{thr}}(z) = (1 - z)^2 \Theta(1 - z), \quad (28)$$

in an analogous form following to Ref. [40]. Taking all the improvements we redefine the SACOT- χ structure function by

$$F_{\phi, \text{thr}}^{\text{SACOT-}\chi}(x, Q^2) \equiv F_{\phi}^{\text{M}}(x, Q^2) + [F_{\phi, \text{thr}}^{\text{ZM-}\chi}(x, Q^2) - F_{\phi, \text{thr}}^{\text{sub-}\chi}(x, Q^2)]. \quad (29)$$

The combination $[F_{\phi, \text{thr}}^{\text{ZM-}\chi} - F_{\phi, \text{thr}}^{\text{sub-}\chi}]$ ensures that the SACOT scheme structure function reduces to massive one near heavy quark threshold. For the SACOT- χ structure function, we always adapt the scale setting $\mu_f = \mu_Q$.

III. NUMERICAL ANALYSIS: STRUCTURE FUNCTIONS

We analyze the structure functions for the scalar interaction. The pseudoscalar case is much the same with scalar case.

A. Effect of χ -rescaling on the structure functions

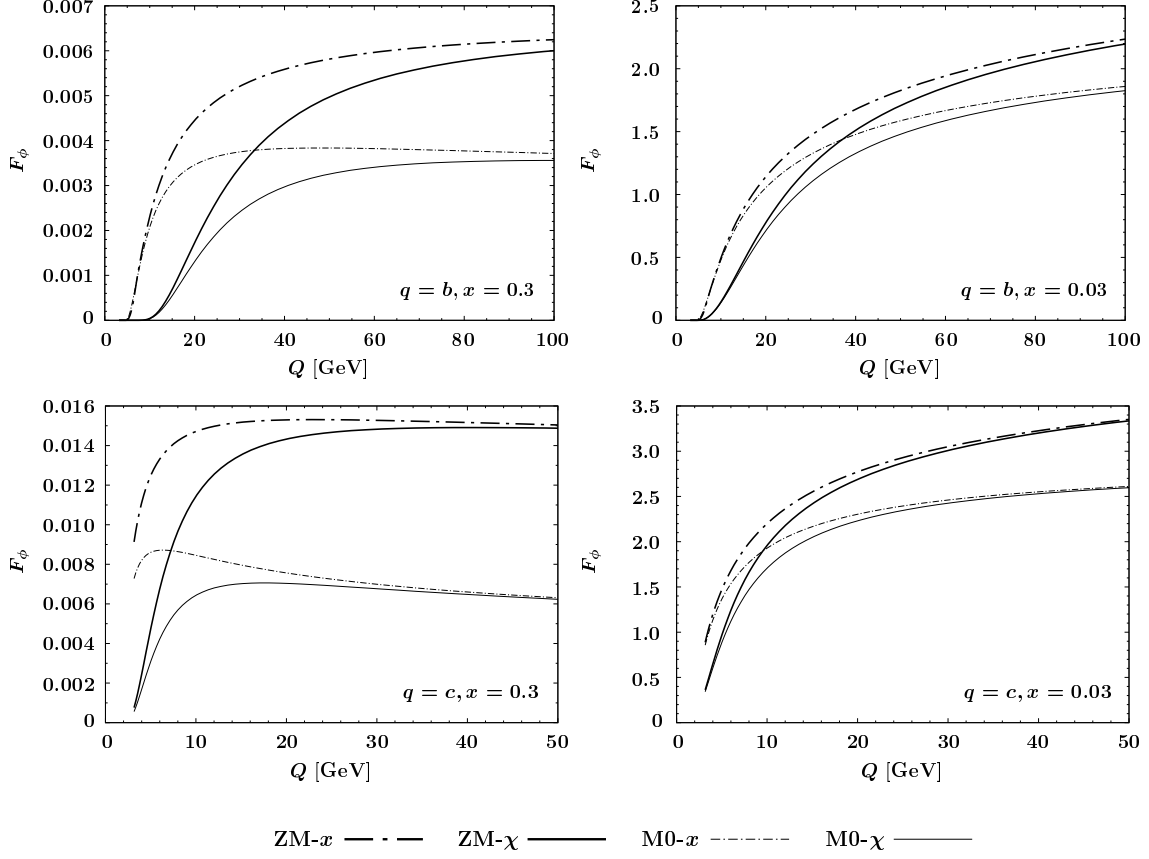


FIG. 5: The structure function F_ϕ computed in the zero-mass scheme with/without χ -rescaling (ZM- χ : Eq.(22)/ ZM- x : Eq.(18)), massless limit of the massive scheme with/without χ -rescaling (M0- χ :Eq.(23)/ M0- x : Eq.(17)) are plotted as functions of Q at $x = 0.3, 0.03$. The upper and lower panels are a contribution of bottom ($q = b$) and charm ($q = c$) quarks, respectively.

Let us first discuss the importance of χ -rescaling for the structure functions in ZM and M0 schemes in the low Q^2 region. The ZM and M0 structure in Eqs.(18) and (17) do not contain any information of the heavy quark threshold in x -scheme. Thus there is no reason to trust the $F_\phi^{\text{ZM-}x}, F_\phi^{\text{M0-}x}$ near heavy quark threshold, while it is expected to have an improvement in χ -rescaling schemes on threshold behavior near $Q \sim m_q$. In Fig.5 ZM and M0 structure functions are plotted as functions of Q . The upper and lower panels are the structure functions for bottom and charm quarks, respectively, for $x = 0.3$ and $x = 0.03$.

The solid lines are ZM- χ , M0- χ structure functions, and dashed lines are corresponding x -scheme structure functions. One can see that the effect of χ -rescaling is huge near heavy quark threshold $Q \sim 2m_q$: $2m_b = 9.5\text{GeV}$ for bottom and $2m_c = 2.6\text{GeV}$ for charm quark. The x -scheme structure functions show unrealistically large even below $Q \leq 2m_q$, and it is remarkable the χ -rescaling improves the unrealistic behavior of the massless structure functions nicely.

The effect of χ -rescaling is decreasing in large Q region, and the difference between use of x or χ -rescaling is negligible, at $Q = 100\text{GeV}$ for bottom quark and $Q = 50\text{GeV}$ for charm quark, compared to the the accuracy of present computation. We conclude that the χ -rescaling is effective only in low Q region in $Q \leq 100, 50\text{GeV}$ for bottom and charm quarks, respectively.

B. Massive vs. ZM, and SACOT scheme

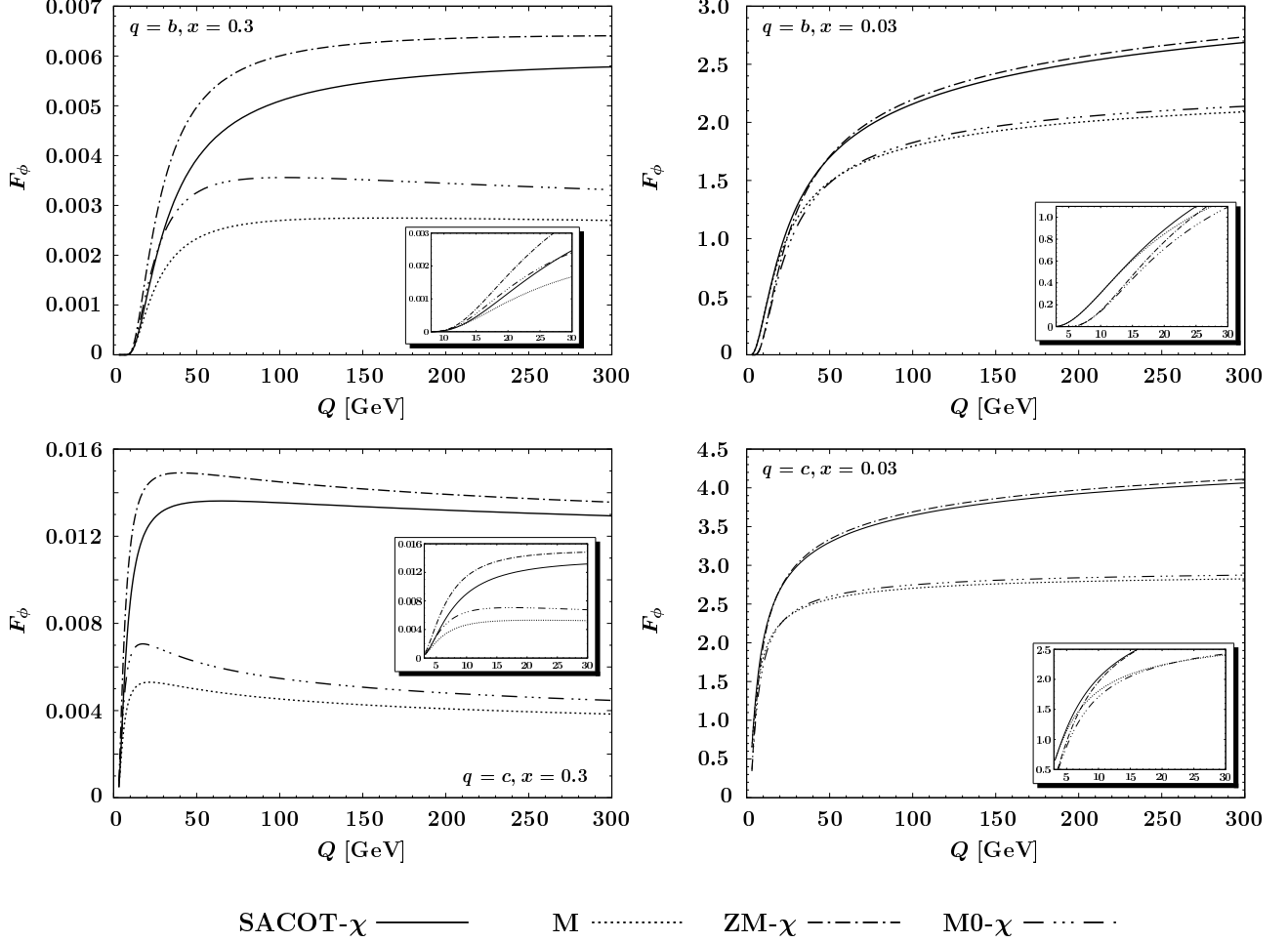


FIG. 6: The structure function F_ϕ computed in the massive scheme (M: Eq.(12)), zero-mass- χ scheme (ZM- χ : Eq.(22)), massless limit of the massive scheme with χ -rescaling (M0- χ : Eq.(23)) and SACOT- χ scheme defined in Eq.(24) are plotted as functions of Q for $x = 0.03, 0.3$. The upper and lower panels are a contribution of bottom ($q = b$) and charm ($q = c$) quarks, respectively.

Here we compare the structure functions in massive, zero-mass and SACOT schemes with χ -rescaling. The scale choice $\mu_f = \mu_Q$ is taken for all the structure functions. In Fig.6 the heavy quark contribution to the structure functions F_ϕ^A , where $A = M, \text{ZM-}\chi, \text{M0-}\chi, \text{SACOT-}\chi$, are plotted as functions of Q for $x = 0.3, 0.03$. For $x = 0.3$ it is seen that

the SACOT- χ and ZM- χ are broadly similar to each others for bottom and charm quarks, and they are much larger than the massive scheme result. The difference between ZM- χ and SACOT- χ is explained by the difference between M and M0- χ because $(F_\phi^{\text{SACOT-}\chi} - F_\phi^{\text{ZM-}\chi}) = (F_\phi^{\text{M}} - F_\phi^{\text{M0-}\chi})$. Remember that M0- χ is the subtraction term of SACOT- χ . For $x = 0.03$ the agreement between SACOT- χ and ZM- χ becomes tighter, because of $(F^{\text{M}} - F^{\text{sub-}\chi})_{x=0.03} \simeq 0$. It should be noted that the structure functions for $x = 0.3$ is three orders of magnitude smaller compared to those of $x = 0.03$.

IV. NUMERICAL ANALYSIS: CROSS SECTIONS

In this section we investigate how effective the SACOT- χ scheme and others are for the description of CLFV process. As is explained in the previous section, the structure functions are functions of x and Q^2 , and each scheme has validity regions for specific Q^2 range. However our concerns are the total cross sections σ and differential distributions $d\sigma/d\mathbf{p}_\tau$ of final τ -momentum. There it arises a question which scheme is the most relevant, and which scheme is the most effective for the description of the CLFV DIS in full kinematical range of the cross section.

For definiteness we take initial and final leptons as electron and tau lepton, respectively, namely $i = e, j = \tau$. In the numerical analysis we ignore electron mass, and take following mass values

$$m_b = 4.75\text{GeV}, \quad m_c = 1.3\text{GeV}, \quad m_\tau = 1.78\text{GeV}. \quad (30)$$

The CLFV couplings ρ_{ij}^ϕ and quark-mediator coupling ρ_{qq}^ϕ are a priori not known and we set their values as

$$|\rho_{qq}^\phi|^2 = (|\rho_{ij}^\phi|^2 + |\rho_{ji}^\phi|^2) = 1. \quad (31)$$

The coupling constants determine the normalization of the CLFV cross section, therefore our numerical results need to be multiplied mode-dependent prefactors to match them with experimental values to be measured. For the choice μ_f we always adapt the $\mu_f = \mu_Q$ defined in Eq. (25). In our numerical analysis we have introduced a kinematical-cut, $Q \geq 1.3\text{GeV}, W \geq 1.4\text{GeV}$ to ensure that the process we are considering is perturbative and deep-inelastic regime, though this is tiny effect and numerically negligible.

A. Zero mass schemes

The ZM schemes were the most frequently used schemes for DIS involving heavy quarks as well as the light quarks. This is so even for CLFV DIS associated with bottom or charm quark production because of its computational simplicity. For low Q^2 the use of massless approximation can not be justified, and a reliable computational scheme should be the massive scheme there. Nevertheless it is worthwhile to know a limitation of the ZM schemes for the CLFV cross sections. Here we investigate ZM- x and ZM- χ schemes to clarify their applicability for the cross section in relatively low collision energies. As example cases we

simulate the cross section for $E_e = 200\text{GeV}$, 1TeV . Here we do not include the threshold factor S_{thr} because it cuts away the low Q region and the difference between ZM- x and ZM- χ are naturally suppressed.

In Fig.7 we show the τ -momentum distribution for CLFV associated with bottom production for $E_e = 200\text{GeV}$ (upper panels) and $E_e = 1\text{TeV}$ (lower panels). The scalar mass is set to $m_s = 10\text{GeV}$. The left and right panels are the distribution in the ZM- x and ZM- χ schemes respectively. Contour lines are labeled by percentages (20, \dots , 80%) of the cross section of enclosed region normalized to their total cross section. The colored region contains 99% of total events. Values of scalar mass m_s , beam energy E_e and the total cross section σ are shown inside each panel. For energy of $E_e = 200\text{GeV}$ an effect of χ -rescaling is huge suppression, and the physical region of χ -scheme distributions are shrunk into a smaller region compared to the those of x -schemes. For $E_e = 1\text{TeV}$ the effect of χ -rescaling is still large for the overall normalization but weaker compared to the case of $E_e = 200\text{GeV}$. The ratio of the total cross section between x and χ schemes is $\sigma_b^{\text{ZM-}x}/\sigma_b^{\text{ZM-}\chi} \sim 70, 3.8$, respectively for $E_e = 200\text{GeV}, 1\text{TeV}$. The large enhancements of the total cross sections in x -schemes hold even in a case of heavy scalar mass. For instance, taking $m_s = 10^5\text{GeV}$, the cross section ratio is $\sigma_b^{\text{ZM-}x}/\sigma_b^{\text{ZM-}\chi} \sim 73, 3.0$ respectively for $E_e = 200\text{GeV}, 1\text{TeV}$ for the bottom quark production.

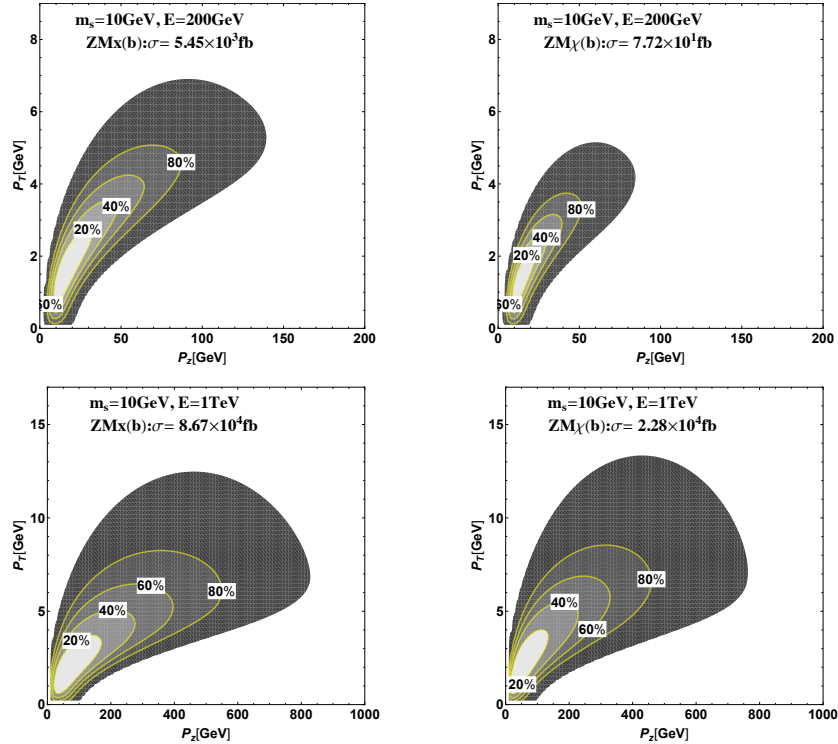


FIG. 7: The τ -momentum distributions for bottom quark production in ZM- x (left panels) or ZM- χ (right panels) schemes. The electron beam energies of $E_e = 200\text{GeV}$ (upper panels) and $E_e = 1\text{TeV}$ (lower panels) with scalar mass $m_s = 10\text{GeV}$ were simulated.

In Fig.8 we show the τ -momentum distributions in case of charm quark production.

Comparing the x and χ schemes shapes of the contour lines look quite similar to each other, but effect of χ -rescaling is still sizable for normalization of the total cross sections. Ratio of the cross sections between x and χ schemes is $\sigma_c^{\text{ZM-}x}/\sigma_c^{\text{ZM-}\chi} \sim 1.7, 1.4$ respectively for $E_e = 200\text{GeV}, 1\text{TeV}$. This value is not change much even for heavy scalar case. For instance, taking $m_s = 10^5\text{GeV}$, the ratio is $\sigma_c^{\text{ZM-}x}/\sigma_c^{\text{ZM-}\chi} \sim 1.6, 1.2$ respectively for $E_e = 200\text{GeV}, 1\text{TeV}$.

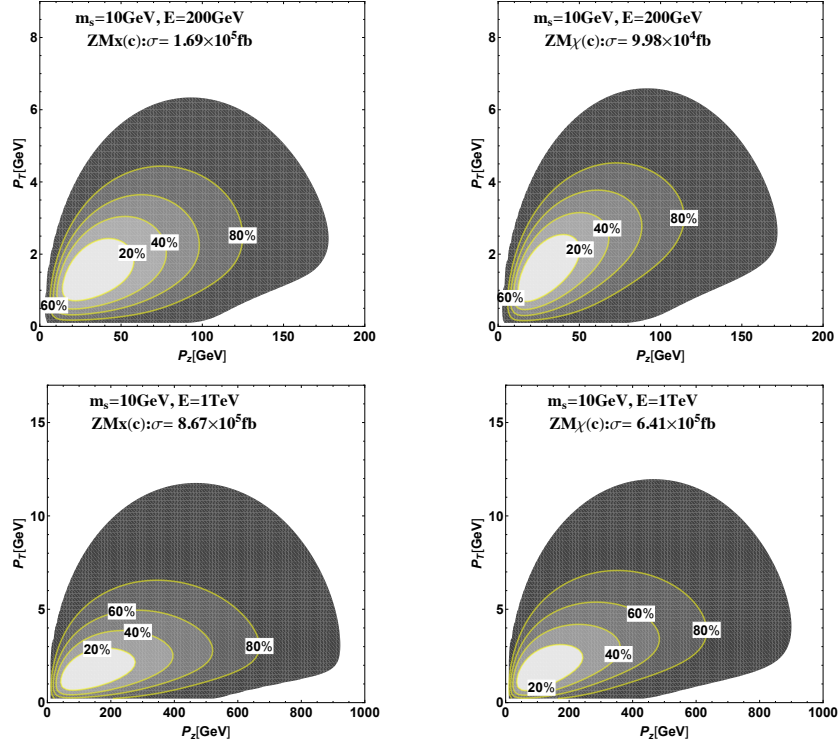


FIG. 8: Same as Fig.7, but heavy quark is charm quark ($q = c$).

In Fig.9 total cross sections associated with bottom quark production are plotted for two cases of scalar mass, $m_s = 10\text{GeV}$ and $m_s = 10^5\text{GeV}$, where each cross section is normalized to the SACOT- χ . Numerical values of the cross sections are listed in Table. I. It can be seen that bottom quark production in the massive scheme is close to the SACOT- χ , $\sigma_{\text{thr,b}}^{\text{M}}/\sigma_{\text{thr,b}}^{\text{SACOT-}\chi} \sim 1$. ZM- χ for the small scalar mass is quite off from SACOT- χ irrespective of the collision energy. For the case of the large scalar mass $m_s = 10^5\text{GeV}$ ZM- χ and ZM- x cross sections are gradually approaching to the SACOT- χ , and around $\sqrt{s} \sim 10^3\text{GeV}$ they meet at one point. It is notable the ZM- x scheme cross section is far off from the SACOT- χ in low collision energy.

The same plot for charm quark production is shown in Fig.10. Even for the charm quark production inadequate of ZM- x scheme in low collision energy is the same, but the behaviors of M and ZM- χ are quite different compared to the bottom cases. For small scalar mass $m_s = 10\text{GeV}$ the massive scheme is growing with \sqrt{s} and overshoot the SACOT- χ , while for large scalar mass $m_s = 10^5\text{GeV}$ it is almost constant and small by a sizable amount compared to SACOT- χ . ZM- χ is close to SACOT- χ for arbitrary collision energy and it is

expected that charm quark can be treated as massless provided that χ -rescaling is adapted for it.

TABLE I: The CLFV total cross sections associated with bottom and charm quark productions in ZM schemes and massive scheme. Here the coupling constants of ϕ with lepton and quarks were set to one (see Eq.(31)).

m_s [GeV]	E_e [GeV]	$\sigma_b^{\text{ZM-}x}$ [fb]	$\sigma_b^{\text{ZM-}\chi}$ [fb]	σ_b^{M} [fb]	$\sigma_c^{\text{ZM-}x}$ [fb]	$\sigma_c^{\text{ZM-}\chi}$ [fb]	σ_c^{M} [fb]
10	10^2	6.49×10^2	1.02×10^{-2}	2.08×10^{-1}	6.57×10^4	2.99×10^4	2.74×10^4
	10^3	8.67×10^4	2.28×10^4	4.93×10^4	8.67×10^5	6.41×10^5	6.59×10^5
	10^4	7.84×10^5	3.72×10^5	7.32×10^5	4.10×10^6	3.46×10^6	4.15×10^6
	10^5	3.24×10^6	1.90×10^6	3.72×10^6	1.15×10^7	1.02×10^7	1.46×10^7
	10^6	9.12×10^6	5.87×10^6	1.18×10^7	2.45×10^7	2.24×10^7	3.83×10^7
	10^7	2.11×10^7	1.43×10^7	2.99×10^7	4.68×10^7	4.33×10^7	8.68×10^7
10^5	10^2	1.51×10^{-13}	2.02×10^{-18}	3.17×10^{-17}	1.00×10^{-11}	4.75×10^{-12}	3.86×10^{-12}
	10^3	5.64×10^{-11}	1.89×10^{-11}	2.23×10^{-11}	3.03×10^{-10}	2.55×10^{-10}	1.93×10^{-10}
	10^4	1.88×10^{-9}	1.41×10^{-9}	1.27×10^{-9}	4.92×10^{-9}	4.70×10^{-9}	3.51×10^{-9}
	10^5	3.35×10^{-9}	3.10×10^{-8}	2.57×10^{-8}	6.37×10^{-8}	6.31×10^{-8}	4.66×10^{-8}
	10^6	4.66×10^{-7}	4.57×10^{-7}	3.66×10^{-7}	7.52×10^{-7}	7.50×10^{-7}	5.48×10^{-7}
	10^6	5.76×10^{-6}	5.73×10^{-6}	4.50×10^{-6}	8.45×10^{-6}	8.45×10^{-6}	6.09×10^{-6}

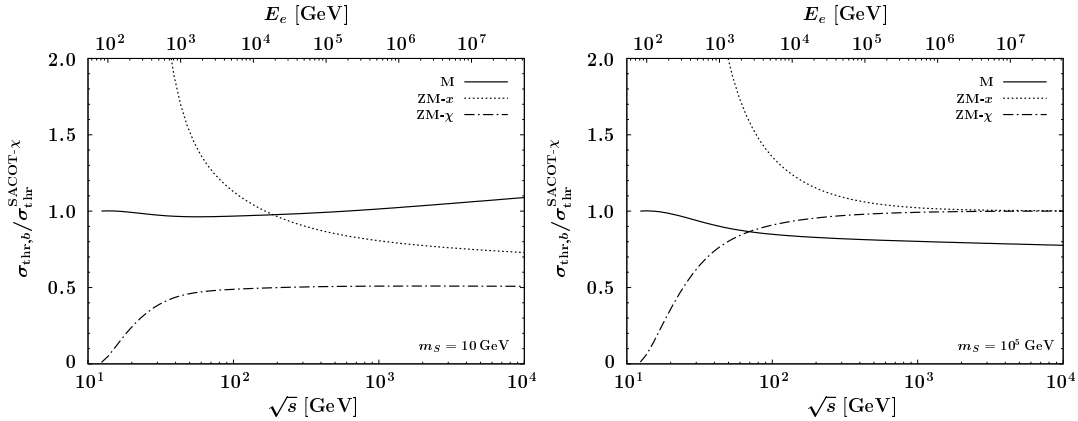


FIG. 9: The CLFV cross sections associated with bottom quark production in M, ZM- x and ZM- χ normalized to SACOT- χ are plotted as functions of \sqrt{s} . Upper horizontal axis is corresponding beam energy of the initial electron in fixed target experiments. The scalar mass is $m_s = 10\text{GeV}$, 10^5GeV respectively in the left and right panels.

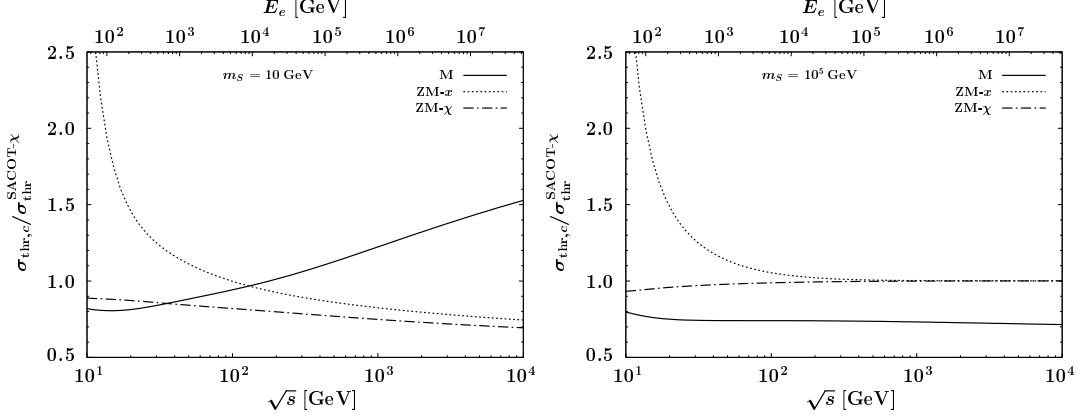


FIG. 10: Same as Fig.9, but for charm quark production.

B. SACOT- χ and its components

In Fig.11 we show the τ -momentum distribution in CLFV DIS associated with bottom quark production in SACOT- χ scheme, where combinations of energies $E = 200\text{GeV}$, 1TeV and the scalar masses $m_s = 10\text{GeV}$, 10^5GeV are shown. For the cross section in SACOT- χ we always adapt the χ -rescaling and threshold factor S_{thr} .

One can see that size of scalar mass does not affect the shape of distribution for $E_E = 200\text{GeV}$, but the overall normalization. For $E_e = 1\text{TeV}$ there is sizable differences in the shape of distribution between $m_s = 10\text{GeV}$ and 10^5GeV . It should be remembered that we have fixed the CLFV couplings by Eq.(31), which could control overall normalization of the cross section. Thus it is of great importance to have a sensitivity to the scalar mass in shape of the distribution, which can be utilized for a detail study to discriminate the structure of the CLFV interactions. Decomposing the cross section of SACOT- χ scheme into M, ZM- χ and M0- χ (=sub- χ one can see the contribution of each component. This is shown in Fig. 12 for the case of $E_e = 1\text{TeV}$ with $m_s = 10\text{GeV}$ or $m_s = 10^5\text{GeV}$. It turns out that the largest contribution is coming from the massive scheme cross section, and the contributions of ZM- χ and M0- χ are the same size. This observation leads that the massive scheme cross section is effective and nearly equal to the SACOT- χ in the range of these collision energies, because ZM- χ and M0- χ cancel each other in the combination of $F^{\text{ZM-}\chi} - F^{\text{sub-}\chi}$. Effectiveness of massive scheme cross section in a wider range collision energy range will be discussed later (see Fig.19 and Fig.20).

In Fig. 13 τ -momentum distribution in CLFV DIS associated with charm quark production is shown for $E_e = 200\text{GeV}$ and $E_e = 1\text{TeV}$. The distribution are more concentrated in high- p_Z region compared to one of bottom quark production because charm quark ($m_c = 1.3\text{GeV}$) is more relativistic than the bottom quark ($m_b = 4.75\text{GeV}$). Again the size of scalar mass appears in the normalization and also shape of the cross section. In the components of SACOT- χ , rate of the massive scheme cross section and ZM- χ are the same size.

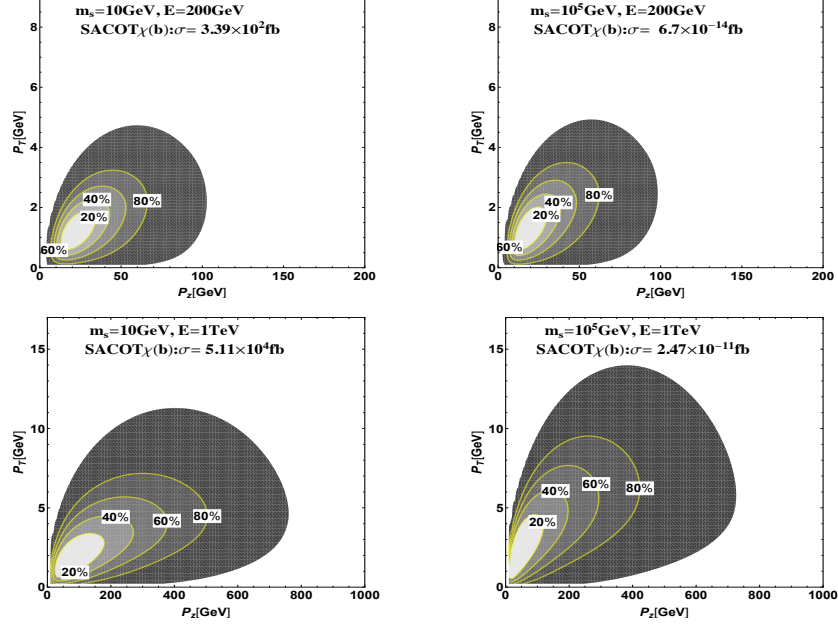


FIG. 11: τ -momentum distribution in CLFV DIS associated with bottom quark production in SACOT- χ scheme with threshold factor S_{thr} implemented. Initial electron beam energy is $E_e = 200\text{GeV}$ and $E_e = 1\text{TeV}$ respectively in upper and lower panels. The scalar mass is $m_s = 10\text{GeV}$, 10^5GeV respectively in left and right panels.

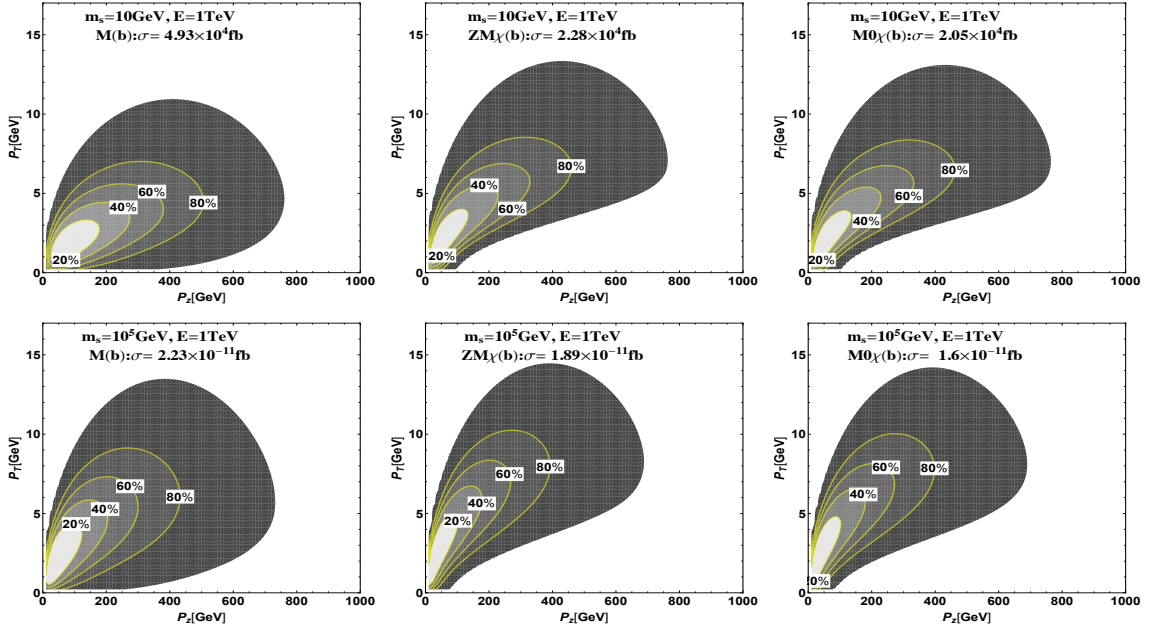


FIG. 12: Components of SACOT- χ scheme, M, ZM- χ , M0- χ without S_{thr} for the τ -momentum distribution. The scalar mass is $m_s = 10\text{GeV}$ and $m_s = 10^5\text{GeV}$ respectively in upper and lower panels, and the initial electron beam is set to $E = 1\text{TeV}$.

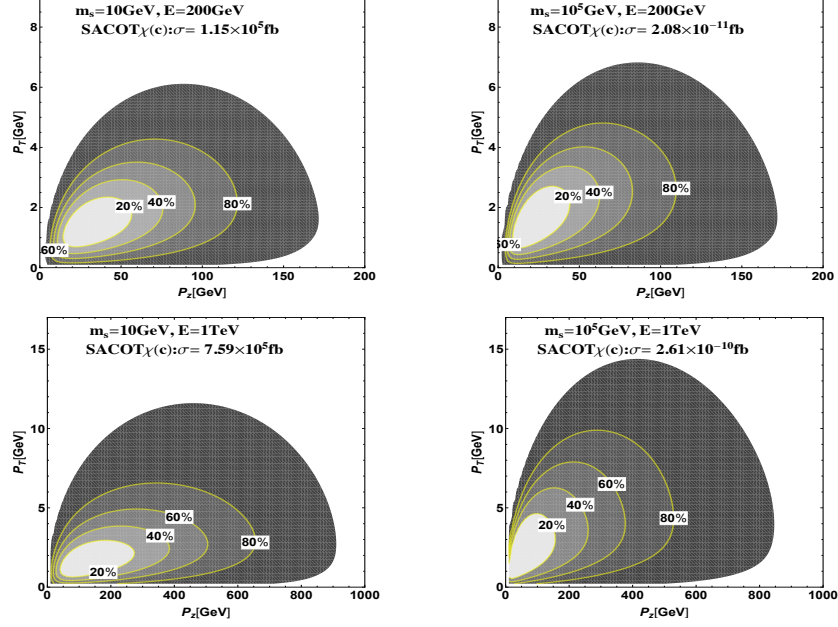


FIG. 13: Same as Fig.11 for charm quark productions.

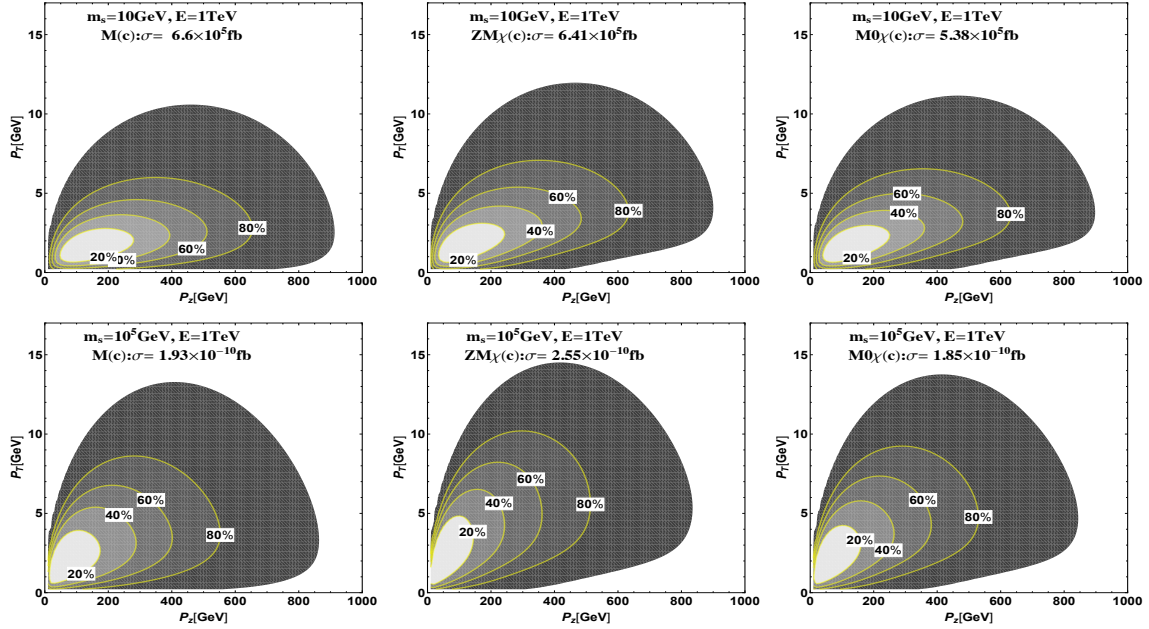


FIG. 14: Same as Fig.12 for charm quark production.

Integrating the structure functions over x one obtain the inverse moments $M_\phi(s, Q^2) = \int x^{-2} F_\phi dx$ defined in Eq.(9). We also define a weighting function W_ϕ by

$$W_\phi(m_\phi^2, Q^2) = \frac{(Q^2)^{\frac{3}{2}}(Q^2 + m_\tau^2)}{8\pi(Q^2 + m_\phi^2)^2}, \quad (32)$$

such that the total cross section is given by $s^2(d\sigma/dQ) = W_\phi(m_\phi^2, Q^2)M_\phi(s, Q^2)$. Note that the definition of the weighting function here gives $d\sigma/dQ$ not $d\sigma/dQ^2$ to make plots as functions of linear scale of Q .

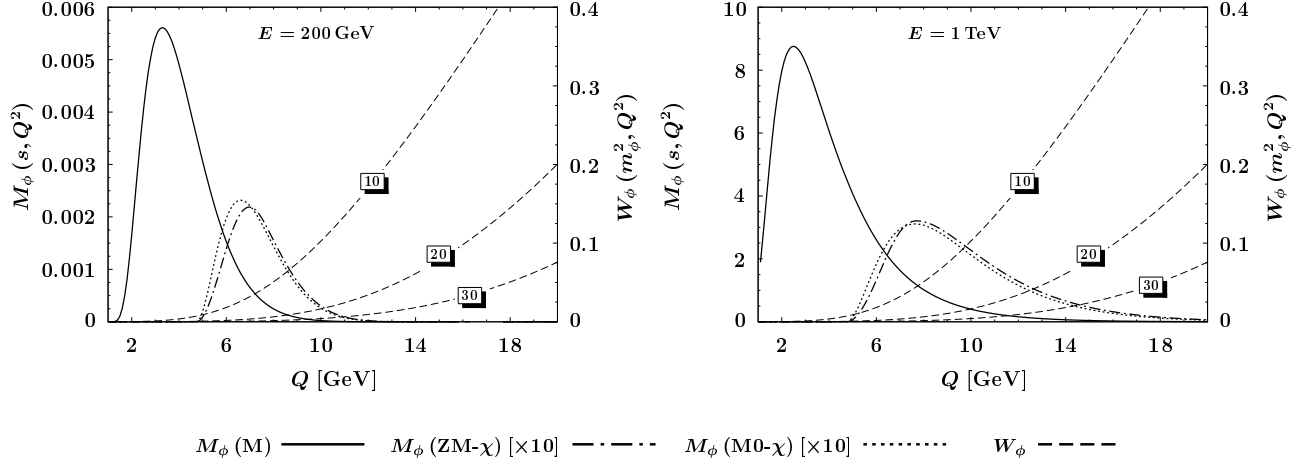


FIG. 15: Inverse moment M_ϕ defined in Eq.(9) of each component of the SACOT- χ structure function for bottom quark and weighting factor W_ϕ defined in Eq.(32). Scalar mass is set to $m_s = 10, 20, 30\text{GeV}$ for $W_\phi(m_s^2, Q^2)$. The left axis and right axis show the ticks for the inverse moment and the weighting function, respectively. Electron beam energy is $E_e = 200\text{GeV}$ and $E_e = 1\text{TeV}$ respectively in the left and right panels. For ZM- χ , M0- χ a factor 10 is multiplied for a visualization.

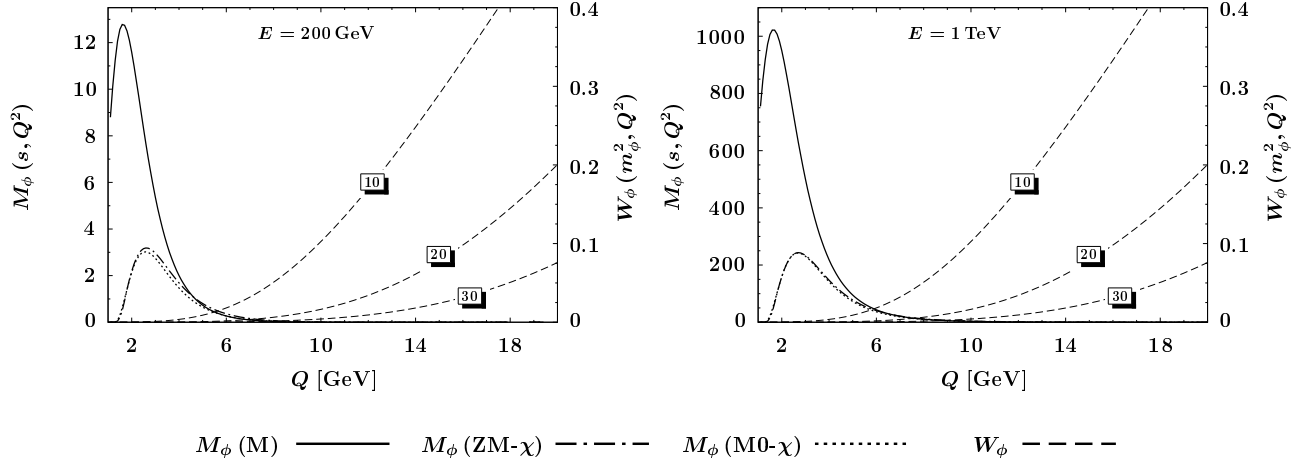


FIG. 16: Same as Fig.15, but for charm quark.

The inverse moment is more adequate than the structure function to see which region of Q is contributing to the cross section. In Figs. 15 and 16, the inverse moments respectively for the bottom and charm quark productions are plotted as function of Q . Note that for ZM- χ and M0- χ of bottom quark are order of magnitude smaller compared to massive scheme ones, and ten times their values are plotted for visualization. In Figs. 17 and 18

$m_\phi^4 \times W_\phi(m_\phi^2, Q^2)M_\phi(s, Q^2)$ are plotted as functions of Q for bottom and charm quark cases. A factor m_s^4 is multiplied to scale out leading m_s -dependence for large m_s behavior.

In the the bottom quark production, the inverse moments of ZM- χ and M0- χ are tiny in magnitude but their support regions are lying in relatively large Q region compared to massive scheme, which leads enhancement by a factor due to weighting function of large Q region. Nevertheless there exists a large cancellation between ZM- χ and M0- χ in the the cross section. Thus effectiveness and dominance of massive scheme cross section is checked from the Q -dependence of the inverse moment in bottom quark production. This is seen in Fig.17, and σ_b^M approximates the SACOT- χ cross section well for $E_e = 200\text{GeV}$ and $E_e = 1\text{TeV}$. In case of charm quark production in Fig.18, it is seen that dominance of the massive scheme cross section does not hold. Actually the cross section in ZM- χ becomes dominant for large scalar mass $m_s = 10^5\text{GeV}$. A breakdown of dominance of the massive scheme cross section occurs depending on the value of scalar mass.

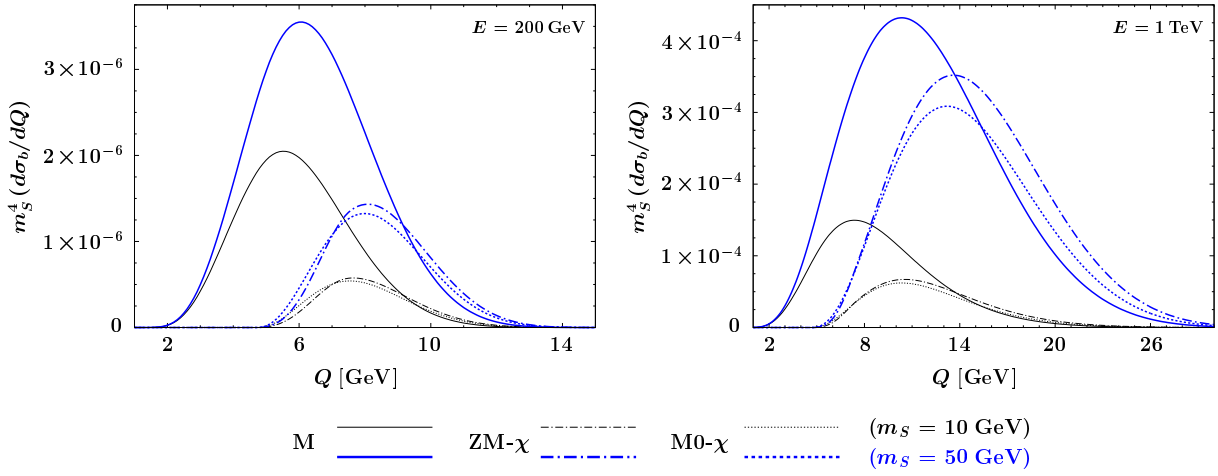


FIG. 17: CLFV cross section associated with bottom quark pair production. Value of cross sections multiplied by m_ϕ^4 is plotted as function of Q . Beam energy is $E_e = 200\text{GeV}$ and $E = 1\text{TeV}$ respectively in left and right panels. The scalar mass is $m_\phi = 10\text{GeV}$ (black lines) and $m_\phi = 50\text{GeV}$ (blue lines).

In Figs.17 and 18 one can see that the subtraction term M0- χ is close to the ZM- χ in low Q region, while in the higher Q it approaches to massive scheme cross section. This is by its construction, that the subtraction term is leading mass singularity of the massive structure function, therefore it interpolates two schemes from low Q to high Q region between zero-mass and massive schemes.

In Fig.19 the dominance of the massive scheme in SACOT- χ cross section holds for $m_s = 10\text{GeV}$ in all the range of \sqrt{s} shown in the plot, but for $m_s = 10^5\text{GeV}$ ZM- χ becomes the dominant component above $\sqrt{s} \sim 10^2\text{GeV}$. The rate of the massive scheme contribution is about 0.8 in high energy. This m_s dependence is interpreted as follows. In the case where the typical momentum transfer is much smaller than the mediator mass $Q^2 \ll m_s^2$, the differential cross section is $d\hat{\sigma}/dx dQ^2 \propto 1/m_s^4$. The Q^2 -integral is approximated by a summation of bars at each Q^2 position with equal-weight, i.e., like a quadrature by parts

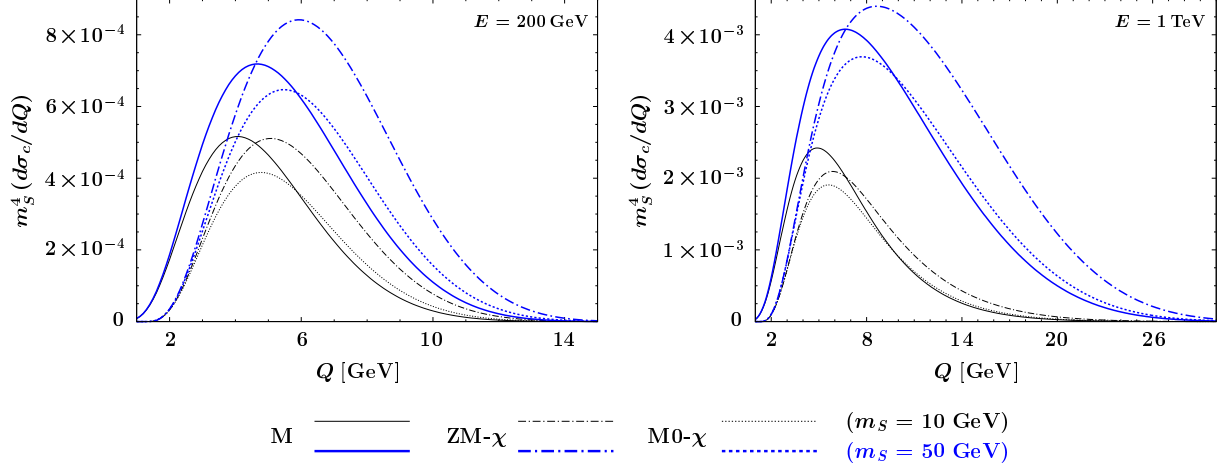


FIG. 18: Same as Fig.17, but for the charm quark production.

for a constant. The large Q^2 component activates heavy flavor PDFs, and makes the ZM description to be reliable. On the other hand, when $Q^2 \gg m_s^2$ or $Q^2 \simeq m_s^2$, $d\hat{\sigma}/dx dQ^2 \propto 1/Q^4$, the small Q^2 part governs the Q^2 -integral. Due to the insufficiency of large Q^2 component, the heavy flavor PDF is not activated.

The same plot for charm quark is shown in Fig.19. For $m_s = 10$ GeV, ZM- χ scheme almost describes the CLFV DIS for all of energy region in this plot. Also for $m_s = 10^5$ GeV, the ZM- χ becomes leading at $\sqrt{s} \sim 10^2$ GeV. As is similar with bottom case, the rate of the massive scheme is about 0.8 in high energy.

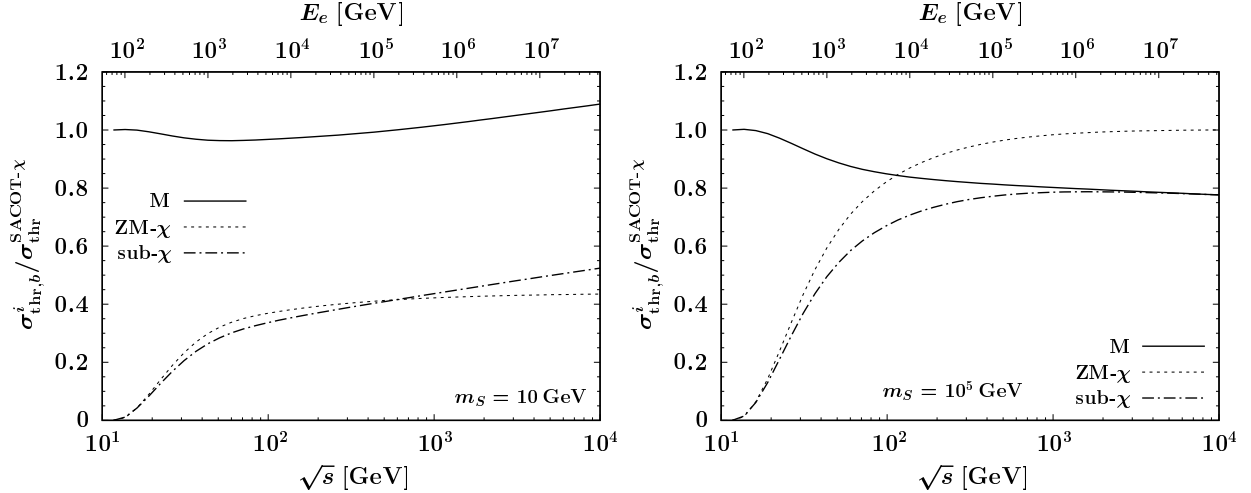


FIG. 19: Comparison among the components of SACOT- χ cross section for CLFV DIS associated with bottom quark production: M, ZM- χ , and M0- χ schemes normalized to SACOT- χ are plotted as function of collision energy \sqrt{s} (upper horizontal axis is the electron beam energy E_e). The scalar mass is set to $m_s = 10$ GeV and $m_s = 10^5$ GeV respectively in the left and right panels.

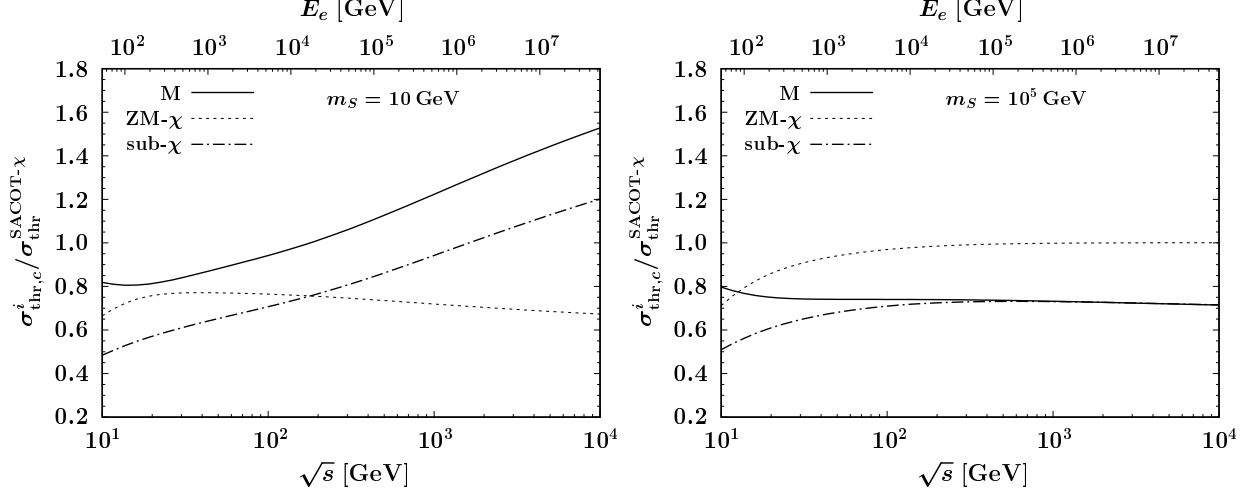


FIG. 20: Same as Fig. 19, but for charm quark production.

TABLE II: The total cross sections for CLFV associated with bottom quark production in SACOT-\$\chi\$ and its components. The ZM-\$\chi\$ M0-\$\chi\$ and SACOT-\$\chi\$ the threshold correction \$S_{thr}\$ is taken into account.

m_s [GeV]	E_e [GeV]	σ_b^M [fb]	$\sigma_{thr,b}^{ZM-\chi}$ [fb]	$\sigma_{thr,b}^{M0-\chi}$ [fb]	$\sigma_{thr,b}^{SACOT-\chi}$ [fb]
10	10^2	2.08×10^{-1}	1.95×10^{-3}	2.32×10^{-3}	2.07×10^{-1}
	10^3	4.93×10^4	1.53×10^4	1.35×10^4	5.11×10^4
	10^4	7.32×10^5	2.87×10^5	2.66×10^5	7.53×10^5
	10^5	3.72×10^6	1.54×10^6	1.51×10^6	3.75×10^6
	10^6	1.18×10^7	4.90×10^6	5.18×10^6	1.15×10^7
	10^7	2.99×10^7	1.22×10^7	1.39×10^7	2.81×10^7
10^5	10^2	3.17×10^{-17}	4.06×10^{-19}	4.74×10^{-19}	3.17×10^{-17}
	10^3	2.23×10^{-11}	1.47×10^{-11}	1.22×10^{-11}	2.47×10^{-11}
	10^4	1.27×10^{-9}	1.32×10^{-9}	1.07×10^{-9}	1.51×10^{-9}
	10^5	2.57×10^{-8}	3.03×10^{-8}	2.44×10^{-8}	3.16×10^{-8}
	10^6	3.66×10^{-7}	4.54×10^{-7}	3.61×10^{-7}	4.59×10^{-7}
	10^7	4.50×10^{-6}	5.72×10^{-6}	4.49×10^{-6}	5.73×10^{-6}

TABLE III: Same as Table II, but for charm quark production.

m_s [GeV]	E_e [GeV]	σ_c^M [fb]	$\sigma_{\text{thr},c}^{\text{ZM-}\chi}$ [fb]	$\sigma_{\text{thr},c}^{\text{M0-}\chi}$ [fb]	$\sigma_{\text{thr},c}^{\text{SACOT-}\chi}$ [fb]
10	10^2	2.74×10^4	2.45×10^4	1.79×10^4	3.40×10^4
	10^3	6.59×10^5	5.85×10^5	4.86×10^5	7.58×10^5
	10^4	4.15×10^6	3.25×10^6	3.13×10^6	4.27×10^6
	10^5	1.46×10^7	9.73×10^6	1.11×10^7	1.32×10^7
	10^6	3.83×10^7	2.15×10^7	2.96×10^7	3.02×10^7
	10^7	8.68×10^7	4.19×10^7	6.78×10^7	6.09×10^7
10^5	10^2	3.86×10^{-12}	3.99×10^{-12}	2.83×10^{-12}	5.03×10^{-12}
	10^3	1.93×10^{-10}	2.43×10^{-10}	1.75×10^{-10}	2.61×10^{-10}
	10^4	3.51×10^{-9}	4.64×10^{-9}	3.41×10^{-9}	4.75×10^{-9}
	10^5	4.66×10^{-8}	6.29×10^{-8}	4.62×10^{-8}	6.33×10^{-8}
	10^6	5.48×10^{-7}	7.50×10^{-7}	5.47×10^{-7}	7.50×10^{-7}
	10^7	6.09×10^{-6}	8.45×10^{-6}	6.09×10^{-6}	8.44×10^{-6}

V. SUMMARY

In this manuscript, we consider a scenario where a CLFV scalar mediator couples dominantly to heavy quarks and extensively study the CLFV DIS $\ell_i N \rightarrow \ell_j X$ processes in a model-independent manner. We conclude that the SACOT- χ prescription is indispensable to predict the reliable sensitivity to the CLFV interactions in the next generation experiments.

One of the most essential CLFV subprocesses is the $\ell_i g \rightarrow \ell_j q \bar{q}$ via the q (or \bar{q}) scattering off the (pseudo-)scalar mediator. We have argued that the heavy quark mass effect is very important to describe the threshold behavior of $q \bar{q}$ production, but the cross section receives the large logarithmic correction due to the mass singularity of $\ln(Q^2/m_q^2)$, which deteriorates the accuracy of the perturbative prediction.

To rescue the reliability of the prediction we applied the so-called SACOT- χ scheme to the CLFV DIS associated with heavy quark production. We derived the heavy flavor structure functions for the (pseudo-)scalar current. The SACOT- χ scheme provides a reliable computational scheme for the CLFV DIS cross section in a wide kinematical regime interpolating the massive scheme to the zero-mass scheme, for which the large logarithmic resummation is available via the DGLAP evolution equation.

We numerically analyzed the each contribution of SACOT scheme and the effect of χ -rescaling in the CLFV DIS associated with heavy quark production.

First, we show the difference between the x -scheme and χ -rescaling in the structure function in Fig. 5 and conclude that the χ -rescaling is effective in $Q \lesssim 100$ (50) GeV for the production of bottom (charm) quark. Therefore, it is necessary to incorporate the χ -rescaling for beam energies of $\lesssim \mathcal{O}(\text{TeV})$ in future experiments. We also found the noticeable differences between the x -scheme and χ -rescaling in cross sections and in the final lepton distributions (Figs. 7 - 10). The x -scheme cross sections does not contain any effect of the heavy quark mass, and it does not show the physical threshold behavior around $Q^2 \sim m_q^2$.

We conclude that if x -scheme were applied to the CLFV DIS processes we would overestimate the event rate of the CLFV signals. Ratio between x and χ schemes is $\sigma_b^{\text{ZM-}x}/\sigma_b^{\text{ZM-}\chi} \simeq 70$ (3) for $E = 200$ GeV (1 TeV) and $m_s = 10^5$ GeV. Thus the quantitative predictions (constraints) on the CLFV DIS processes require the χ -rescaling.

Next, we numerically demonstrated the effect of the SACOT- χ scheme. Figs. 19 and 20 showed the importance of SACOT- χ scheme. The simple calculation employs the subprocess $\ell_i q \rightarrow \ell_j q$ using heavy flavor PDFs, which is labeled by ZM- χ . Depending on the mediator mass, the beam energy, and the flavor of heavy quarks, this simple calculation breaks down. In some cases, ZM- χ and M scheme give the comparable contributions, and only the SACOT- χ scheme results in a reliable prediction for the CLFV DIS cross section.

Finally, we have discussed the mediator mass dependences on the CLFV DIS observables. We considered the two representative cases, i.e., much lighter and heavier masses compared with the typical momentum transfer; $m_s = 10$ GeV and $m_s = 10^5$ GeV. We found that, for a fixed beam energy, the ratio of the contributions from the massive and the zero-mass scheme strongly depends on the mediator mass. This is because when the mediator mass is small, the contributions from the small Q^2 region is enhanced. Therefore, using the momentum distributions in the CLFV DIS processes we can probe the mass of the CLFV mediator.

Other types of subprocesses contribute to the CLFV DIS process via the gluonic operator $\ell_i g \rightarrow \ell_j g$ and the photonic dipole operator $\ell_i q_l \rightarrow \ell_j q_l$ (here q_l stands for a light flavor quarks). The comprehensive analysis of the DIS observables taking these subprocesses into account enables both to disentangle the type of the CLFV operators and to unravel the CLFV mediators. We leave these issues for our future works.

Acknowledgements

This work was partly supported by MEXT Joint Usage/Research Center on Mathematics and Theoretical Physics JPMXP0619217849 (M.Y.), JSPS KAKENHI Grant Numbers JP18H01210 and JP21H00081 (Y.U.) and the JSPS Grant-in-Aid for Scientific Research No. 18K03611, 16H06492 and 20H00160(M.T.).

Appendix A: Physical region of DIS kinematics

1. Range of (x, y) in generic case

We derive the physical region of kinematical variable x, y for CLFV DIS process $\ell_i(k_i)p(p) \rightarrow \ell_j(k_j)x(p_x)$. We assume that the initial QCD parton p is massless with momentum $p = \xi P$, and other particles are massive: $k_i^2 = m_i^2, p^2 = 0, k_j^2 = m_j^2, p_x^2 = w^2$. Similar analysis can be found in literatures [48, 49].

First we express the kinematical variables in CM frame of lepton and parton, where lepton energies are given by

$$E_i = \frac{\hat{s} + m_i^2}{2\sqrt{\hat{s}}}, \quad E_j = \frac{\hat{s} + m_j^2 - w^2}{2\sqrt{\hat{s}}}, \quad (\text{A1})$$

where $\hat{s} = (p + k_i)^2$ is related to the lepton-nucleon collision energy squared $s = (P + k_i)^2$ by $\hat{s} - m_i^2 = \xi(s - m_i^2)$. The momentum transfer $Q^2 = -(k_i - k_j)^2$ in CM frame is given by $Q^2 = -(m_j^2 + m_i^2) + 2E_i E_j - 2|\mathbf{k}_i||\mathbf{k}_j|\cos\theta_{ij}$. The spacial momentum of leptons can be replaced by $|\mathbf{k}_i||\mathbf{k}_j| = \sqrt{E_i^2 - m_i^2}\sqrt{E_j^2 - m_j^2}$. With the expression the angle θ_{ij} is written as

$$\cos\theta_{ij} = \frac{2E_i E_j - xy(s - m_i^2) - (m_i^2 + m_j^2)}{2\sqrt{E_i^2 - m_i^2}\sqrt{E_j^2 - m_j^2}}, \quad (\text{A2})$$

where $Q^2 = xy(s - m_i^2)$ is used. The constraint $|\cos\theta_{ij}| \leq 1$ leads to an inequality

$$[2E_i E_j - xy(s - m_i^2) - (m_i^2 + m_j^2)]^2 \leq 4(E_i^2 - m_i^2)(E_j^2 - m_j^2) \quad (\text{A3})$$

Substituting the lepton energies by Eq.(A1), we obtain

$$y \{ (1 - y)[x(s - m_i^2) + m_i^2] - m_j^2 \} \geq 0, \quad (\text{A4})$$

where we used $w^2 = (p + q)^2 = y(\hat{s} - m_i^2)(1 - x/\xi)$. This condition determines the upper bound of the inelasticity y

$$y \leq 1 - \frac{r_j}{x + r_i}, \quad (\text{A5})$$

Here we introduced dimensionless masses r_a ($a = i, j, w$)

$$r_i = \frac{m_i^2}{s - m_i^2}, \quad r_j = \frac{m_j^2}{s - m_i^2}, \quad r_w = \frac{w^2}{s - m_i^2}. \quad (\text{A6})$$

The lower one is bound by the partonic phase space. We express the inelasticity parameter y in terms of x and w^2

$$y = \frac{1}{\xi - x} \left(\frac{w^2}{s - m_i^2} \right). \quad (\text{A7})$$

The momentum fraction ξ is expressed in terms of Lorentz invariance as $\xi = x (Q^2 + \omega^2) / Q^2$, and its minimum needs to be less than x ;

$$\xi = x \left(\frac{Q^2 + w_{\min}^2}{Q^2} \right) \geq x. \quad (\text{A8})$$

Thus the lower bound of y is given by the production threshold of w_{\min}^2 with maximum momentum fraction $\xi = 1$:

$$y \geq \frac{1}{1-x} \left(\frac{w_{\min}^2}{s - m_i^2} \right) \quad (\text{A9})$$

Thus physical range of y for fixed x is given by $y_{\min} \leq y \leq y_{\max}$ with

$$y_{\min}(x) = \frac{r_{\min}}{1-x}, \quad y_{\max}(x) = 1 - \frac{r_j}{x + r_i}, \quad (\text{A10})$$

where $r_{\min} \equiv w_{\min}^2 / (s - m_i^2)$.

The physical range of x can be obtained by requiring that the lower bound on y should be smaller than the upper one, namely $y_{\min}(x) \leq y_{\max}(x)$ should holds. Their constraint yields a relation

$$x^2 - (1 - r_i + r_j - r_{\min})x - (r_i - r_j - r_i r_{\min}) \leq 0. \quad (\text{A11})$$

Solving the quadratic equation for x , we find the range $x_- \leq x \leq x_+$ with

$$x_{\pm} = \frac{1}{2} \left[(1 - r_i + r_j - r_{\min}) \pm \sqrt{(1 - r_i + r_j - r_{\min})^2 + 4(r_i - r_j - r_i r_{\min})} \right]. \quad (\text{A12})$$

2. Heavy quark pair production in terms of (x, y)

Here we given concrete expression for the physical region by taking initial and final leptons as electron and tau, and in the hadronic part heavy quark pair of mass m_q . We ignore the electron mass, but tau and heavy quark masses are kept. In this case the Eq.(A10) reduces to

$$y_{\min}(x) = \frac{4m_q^2}{(1-x)s}, \quad y_{\max}(x) = 1 - \frac{m_{\tau}^2}{xs}, \quad (\text{A13})$$

and Eq.(A12)

$$x_{\pm} = \frac{1}{2} \left[1 + \frac{m_{\tau}^2}{s} - \frac{4m_q^2}{s} \pm \sqrt{\left(1 + \frac{m_{\tau}^2}{s} - \frac{4m_q^2}{s} \right)^2 - 4 \frac{m_{\tau}^2}{s}} \right], \quad (\text{A14})$$

where minimum of invariant hadronic mass of heavy quark pair is given by $w_{\min}^2 = 4m_q^2$.

3. Heavy quark pair production in terms of (x, Q^2)

When one takes (x, Q^2) as independent variables instead of (x, y) , the relation $xy = Q^2/s$ can be used. The physical region for x is given by $x_{\min}(s, Q^2) \leq x \leq x_{\max}(Q^2)$ with

$$x_{\min}(s, Q^2) = \frac{Q^2 + m_\tau^2}{s}, \quad x_{\max}(Q^2) = \frac{Q^2}{Q^2 + 4m_q^2}, \quad (\text{A15})$$

and for Q^2 the physical region is $Q_-^2 \leq Q^2 \leq Q_+^2$ with

$$Q_\pm^2 = sx_\pm - m_\tau^2, \quad (\text{A16})$$

where x_\pm is defined in Eq.(A14).

-
- [1] Y. Kuno and Y. Okada, Rev. Mod. Phys. **73**, 151 (2001), hep-ph/9909265.
 - [2] M. Raidal et al., Eur. Phys. J. **C57**, 13 (2008), 0801.1826.
 - [3] S. J. Huber, Nucl. Phys. **B666**, 269 (2003), hep-ph/0303183.
 - [4] G. Moreau and J. Silva-Marcos, JHEP **03**, 090 (2006), hep-ph/0602155.
 - [5] K. Agashe, A. E. Blechman, and F. Petriello, Phys. Rev. D **74**, 053011 (2006), hep-ph/0606021.
 - [6] S. Davidson, G. Isidori, and S. Uhlig, Phys. Lett. **B663**, 73 (2008), 0711.3376.
 - [7] S. Kanemura, T. Ota, and K. Tsumura, Phys. Rev. D **73**, 016006 (2006), hep-ph/0505191.
 - [8] S. Davidson and G. J. Grenier, Phys. Rev. D **81**, 095016 (2010), 1001.0434.
 - [9] F. Botella, G. Branco, M. Nebot, and M. Rebelo, Eur. Phys. J. C **76**, 161 (2016), 1508.05101.
 - [10] K. Tsumura and L. Velasco-Sevilla, Phys. Rev. D **81**, 036012 (2010), 0911.2149.
 - [11] S. N. Gninenko, M. M. Kirsanov, N. V. Krasnikov, and V. A. Matveev, Mod. Phys. Lett. **A17**, 1407 (2002), hep-ph/0106302.
 - [12] M. Sher and I. Turan, Phys. Rev. **D69**, 017302 (2004), hep-ph/0309183.
 - [13] S. Kanemura, Y. Kuno, M. Kuze, and T. Ota, Phys. Lett. **B607**, 165 (2005), hep-ph/0410044.
 - [14] M. Gonderinger and M. J. Ramsey-Musolf, JHEP **11**, 045 (2010), [Erratum: JHEP 05, 047 (2012)], 1006.5063.
 - [15] A. Bolanos, A. Fernandez, A. Moyotl, and G. Tavares-Velasco, Phys. Rev. D **87**, 016004 (2013), 1212.0904.
 - [16] W. Liao and X.-H. Wu, Phys. Rev. D **93**, 016011 (2016), 1512.01951.
 - [17] A. Abada, V. De Romeri, J. Orloff, and A. Teixeira, Eur. Phys. J. C **77**, 304 (2017), 1612.05548.
 - [18] M. Takeuchi, Y. Uesaka, and M. Yamanaka, Phys. Lett. **B772**, 279 (2017), 1705.01059.
 - [19] S. Gninenko, S. Kovalenko, S. Kuleshov, V. E. Lyubovitskij, and A. S. Zhevlakov, Phys. Rev. D **98**, 015007 (2018), 1804.05550.
 - [20] S. Antusch, A. Hammad, and A. Rashed, Phys. Lett. B **810**, 135796 (2020), 2003.11091.
 - [21] T. Husek, K. Monsalvez-Pozo, and J. Portoles, JHEP **01**, 059 (2021), 2009.10428.
 - [22] V. Cirigliano, K. Fuyuto, C. Lee, E. Mereghetti, and B. Yan, JHEP **03**, 256 (2021), 2102.06176.

- [23] S. Antusch, A. Hammad, and A. Rashed, JHEP **03**, 230 (2021), 2010.08907.
- [24] O. Cakir, A. Senol, and A. Tasci, EPL **88**, 11002 (2009), 0905.4347.
- [25] T. Han and B. Mellado, Phys. Rev. **D82**, 016009 (2010), 0909.2460.
- [26] H. Liang, X.-G. He, W.-G. Ma, S.-M. Wang, and R.-Y. Zhang, JHEP **09**, 023 (2010), 1006.5534.
- [27] C. Blaksley, M. Blennow, F. Bonnet, P. Coloma, and E. Fernandez-Martinez, Nucl. Phys. B **852**, 353 (2011), 1105.0308.
- [28] S. S. Biswal, R. M. Godbole, B. Mellado, and S. Raychaudhuri, Phys. Rev. Lett. **109**, 261801 (2012), 1203.6285.
- [29] S. Dutta, A. Goyal, M. Kumar, and B. Mellado, Eur. Phys. J. **C75**, 577 (2015), 1307.1688.
- [30] R. Li, X.-M. Shen, K. Wang, T. Xu, L. Zhang, and G. Zhu, Phys. Rev. **D97**, 075043 (2018), 1711.05607.
- [31] D. Curtin, K. Deshpande, O. Fischer, and J. Zurita, JHEP **07**, 024 (2018), 1712.07135.
- [32] S.-Y. Li, Z.-G. Si, and X.-H. Yang, Phys. Lett. B **795**, 49 (2019), 1811.10313.
- [33] G. Azuelos, M. D’Onofrio, S. Iwamoto, and K. Wang, Phys. Rev. D **101**, 095015 (2020), 1912.03823.
- [34] A. Aktas et al. (H1), Eur. Phys. J. C **52**, 833 (2007), hep-ex/0703004.
- [35] F. Aaron et al. (H1), Phys. Lett. B **701**, 20 (2011), 1103.4938.
- [36] A. Accardi et al., Eur. Phys. J. A **52**, 268 (2016), 1212.1701.
- [37] J. L. Abelleira Fernandez et al. (LHeC Study Group), J. Phys. **G39**, 075001 (2012), 1206.2913.
- [38] M. A. G. Aivazis, J. C. Collins, F. I. Olness, and W.-K. Tung, Phys. Rev. **D50**, 3102 (1994), hep-ph/9312319.
- [39] M. Cacciari, M. Greco, and P. Nason, JHEP **05**, 007 (1998), hep-ph/9803400.
- [40] S. Forte, E. Laenen, P. Nason, and J. Rojo, Nucl. Phys. B **834**, 116 (2010), 1001.2312.
- [41] V. N. Gribov and L. N. Lipatov, Sov. J. Nucl. Phys. **15**, 438 (1972).
- [42] G. Altarelli and G. Parisi, Nucl. Phys. B **126**, 298 (1977).
- [43] S. Dulat, T.-J. Hou, J. Gao, M. Guzzi, J. Huston, P. Nadolsky, J. Pumplin, C. Schmidt, D. Stump, and C. P. Yuan, Phys. Rev. D **93**, 033006 (2016), 1506.07443.
- [44] W.-K. Tung, S. Kretzer, and C. Schmidt, J. Phys. G **28**, 983 (2002), hep-ph/0110247.
- [45] S. Kretzer, H. L. Lai, F. I. Olness, and W. K. Tung, Phys. Rev. D **69**, 114005 (2004), hep-ph/0307022.
- [46] R. M. Barnett, Phys. Rev. Lett. **36**, 1163 (1976).
- [47] M. Krämer, F. I. Olness, and D. E. Soper, Phys. Rev. D **62**, 096007 (2000), hep-ph/0003035.
- [48] C. H. Albright and C. Jarlskog, Nucl. Phys. **B84**, 467 (1975).
- [49] K. Hagiwara, K. Mawatari, and H. Yokoya, Nucl. Phys. **B668**, 364 (2003), [Erratum: Nucl. Phys. B701,405(2004)], hep-ph/0305324.